

Mapping the SMEFT to discoverable models

Ricardo Cepedello,^a Fabian Esser,^b Martin Hirsch^b and Veronica Sanz^{b,c}

^a*Institut für Theoretische Physik und Astrophysik, Universität Würzburg, 97074 Würzburg, Germany*

^b*Instituto de Física Corpuscular (IFIC), Universidad de Valencia-CSIC, E-46980 Valencia, Spain*

^c*Department of Physics and Astronomy, University of Sussex, Brighton BN1 9QH, UK*

E-mail: ricardo.cepедello@physik.uni-wuerzburg.de, esser@ific.uv.es,
mahirsch@ific.uv.es, veronica.sanz@uv.es

ABSTRACT: The matching of specific new physics scenarios onto the SMEFT framework is a well-understood procedure. The inverse problem, the matching of the SMEFT to UV scenarios, is more difficult and requires the development of new methods to perform a systematic exploration of models. In this paper we use a diagrammatic technique to construct in an automated way a complete set of possible UV models (given certain, well specified assumptions) that can produce specific groups of SMEFT operators, and illustrate its use by generating models with no tree-level contributions to four-fermion (4F) operators. Those scenarios, which only contribute to 4F at one-loop order, can contain relatively light particles that could be discovered at the LHC in direct searches. For this class of models, we find an interesting interplay between indirect SMEFT and direct searches. We discuss some examples on how this interplay would look like when combining low-energy observables with the SMEFT Higgs-fermion analyses and searches for resonance at the LHC.

KEYWORDS: SMEFT, UV completions, LHC physics, precision observables

Contents

1	Introduction	1
2	One-loop models for SMEFT 4F operators	3
2.1	From operators to models	3
2.2	Restrictions for LHC-testable UV models	8
2.3	Tree-level $\psi^2 H^2 D$ and $\psi^2 H^3$ operators	10
3	Model candidates and their matching to 4F operators	11
3.1	Counting UV completions	11
3.2	Patterns in SMEFT 4F operators	15
3.3	New particles running in loop-induced 4F operators	17
3.4	Minimal scenarios and their explicit matching	18
3.5	Non-minimal quark-specific scenarios	23
4	The phenomenological interplay between SMEFT indirect limits and direct searches at the LHC	23
4.1	Indirect searches with precise low-energy data	23
4.2	Direct high-energy probes	24
4.3	The interplay between low-energy and LHC resonant probes	25
5	Conclusions	27
A	Quark specific models	28

1 Introduction

In high-energy physics we search for new heavy states through direct production of resonances at colliders or indirectly via precision measurements, sensitive to virtual effects from these states. Indirect searches for new physics are often analysed in the context of an Effective Field Theory (EFT) approach, and nowadays the most widely used EFT approach is labelled as SMEFT, or SM EFT [1–12].

On the precision frontier, a legacy of LEP e^+e^- collision measurements, plus other low energy probes such as atomic parity, provide very stringent constraints on new states, see for example analyses using low-energy precision data [13–15]. Even assuming a minimal flavour violation structure of couplings, indirect constraints seem to push the boundary of new physics into the multi-TeV region.

With such high scales, the LHC may have no chance to directly produce the resonances and could only be sensitive again to indirect probes. Indeed, a lot of the current focus using

SM LHC precision measurements is placed in SMEFT analyses combining various LHC channels, as well as legacy measurements at lower energies. Here again the constraints from global fits including legacy and LHC Run2 data place bounds on the scale of dimension-six operators in the multi-TeV range, see [16] for the most up-to-date analysis using LHC Higgs, diboson and top data.

The argument that legacy precision measurements point to a high new physics scale, inaccessible via direct searches, is clearly scenario-dependent. Having a closer look to this issue, one notices that the tightest SMEFT bounds come from a particular set of EFT operators, namely those involving four fermions (4F), particularly those 4F with at least some leptons. Indeed, constraints on flavour-independent 4F operators range from percent to permille level [14]. (We note that it is well-known that constraints on generation off-diagonal entries in the 4F operators are even more stringent, in particular for operators containing leptons [17]. Thus, in all of this paper we will consider only the generation diagonal parts of the operator, as is usually done in LHC analysis.) Therefore, new resonances producing 4F operators at tree-level are constrained to mass regions of the order of $m > \lambda^2 \times (\text{multi-TeV})$, with λ the coupling of the state to the SM fermions.

This conclusion is correct, of course, only if the new states produce the 4F operators at tree-level. On the other hand, in scenarios where 4F are loop-induced at leading order the constraints would be reduced by a factor of order $1/16\pi^2$. Then the new resonances could be much lighter, directly accessible at colliders. In this class of scenarios, information from low-energy precision measurements and collider searches would be complementary.

A systematic description of such *discoverable* scenarios is the focus of this paper. Now, given a particular non-renormalisable operator, it is in principle straightforward to find some particular field (or fields) beyond the Standard Model particle content that will generate the operator in the EFT limit. Due to the finite number of operators in SMEFT at $d = 6$, it is even possible to find the complete list of such ultra-violet, renormalisable completions “by hand”, if one restricts the search to tree-level diagrams [18].¹ However, already at one-loop level the number of possible ultra-violet completions (“models”) increases so rapidly that for any attempt to systematically classify them, automation becomes mandatory.

The strategy we use in this paper for this task is based on a diagrammatic method. We will discuss the basics of this method in section 2. The same method was used previously in the deconstruction of the $d = 5$ Weinberg operator, see [21, 22] and in particular [23]. Note that our method for operator deconstruction overlaps in considerable parts with the one discussed recently in [24–26]. The diagrammatic method can be formulated in a general way, such that one can, in principle, “deconstruct” or “explode”² any EFT operator at arbitrary dimension. For reasons discussed above, however, in this paper we concentrate on 4F operators in SMEFT only.

The paper is organised as follows: In section 2 we present the main ideas of the diagrammatic method we have developed to systematically find loop-induced 4F operators and

¹Some attempts on constructing UV complete models for the SMEFT at $d = 7$ and $d = 8$ have been made in [19], although one should note this work is not fully consistent with previous works, e.g. Ref. [20].

²Finding the UV completion for operators has been called “exploding” the operators in [27].

describe conditions to further restrict the UV scenarios. In section 3 we count the number of UV completions, describe common patterns among these models, propose a benchmark for analysing the phenomenology and explore scenarios that lead to 4F with just quarks, see also Appendix A. In section 4 we use the model patterns to describe the typical phenomenology at the LHC and give specific predictions for our benchmark model. We finish by presenting our conclusions in section 5.

2 One-loop models for SMEFT 4F operators

In this section we discuss the construction of one-loop models for SMEFT 4F operators. The well-known list of baryon and lepton number conserving operators in the Warsaw basis is given in table 1. As mentioned above, while at tree-level there is a small and fixed number of UV completions, at one-loop level a huge number of valid models can be constructed. In subsection 2.1 we briefly describe how we construct the list of models in an automated way. Since in this work we are mainly interested in models testable at the LHC, we will apply a number of restrictions on the list of models. These will be discussed in subsection 2.2.

2.1 From operators to models

Here, we give a brief summary of the diagrammatic method, for further details see [23]. The method involves essentially three steps. For any given operator, one can first find all topologies with n external legs and k loops. Since the aim is to find renormalisable UV models, only topologies with 3- and 4-point vertices are kept. Into these topologies one then inserts fermions, scalars and vectors in all possible ways allowed by Lorentz invariance to find the complete list of diagrams.

Figure 1 outlines how the procedure works schematically for the example of 4F operators. The upper half of the figure shows the tree-level case. For this simple operator at tree-level there are only two topologies. The second of these involves a single four point vertex, and thus, for fermions, is a non-renormalisable vertex. This topology is therefore immediately discarded as we are interested in UV renormalisable models. The first topology can be realised by only two diagrams, which are shown below the topologies. At one-loop level, there are already nine topologies, but again five of those can be thrown away immediately in the case of a 4F operator since they contain 4-point vertices connected to the outside of the topology. Of the remaining four topologies, the one in the last line of topologies is a self-energy that only renormalises the propagator of one of the outside fermions. We will not discuss this topology further here, see the discussion on matching below. This leaves the three topologies in the first line for further study. As in the case of the tree-level, one can now insert fermions, scalars and vectors into the topologies in all physically consistent ways. Note that the figure shows only a few diagrams for the box topology, the list of diagrams shown in this figure is not complete at one-loop order. Both steps can be automatised easily, since mathematically topologies and diagrams can be represented in terms of adjacency matrices. In these adjacency matrices rows and columns represent each vertex, so they should be renormalisable and allowed by Lorentz invariance. We have implemented this procedure in `Mathematica`.

Class	Name	Structure
LL	\mathcal{O}_{ll}	$(\bar{l}_L \gamma_\mu l_L) (\bar{l}_L \gamma^\mu l_L)$
	\mathcal{O}_{le}	$(\bar{l}_L \gamma_\mu l_L) (\bar{e}_R \gamma^\mu e_R)$
	\mathcal{O}_{ee}	$(\bar{e}_R \gamma_\mu e_R) (\bar{e}_R \gamma^\mu e_R)$
LQ	$\mathcal{O}_{lq}^{(1)}$	$(\bar{l}_L \gamma_\mu l_L) (\bar{q}_L \gamma^\mu q_L)$
	$\mathcal{O}_{lq}^{(3)}$	$(\bar{l}_L \gamma_\mu \sigma_a l_L) (\bar{q}_L \gamma^\mu \sigma_a q_L)$
	\mathcal{O}_{lu}	$(\bar{l}_L \gamma_\mu l_L) (\bar{u}_R \gamma^\mu u_R)$
	\mathcal{O}_{ld}	$(\bar{l}_L \gamma_\mu l_L) (\bar{d}_R \gamma^\mu d_R)$
	$\mathcal{O}_{lequ}^{(1)}$	$(\bar{l}_L e_R) i\sigma_2 (\bar{q}_L u_R)^T$
	$\mathcal{O}_{lequ}^{(3)}$	$(\bar{l}_L \sigma_{\mu\nu} e_R) i\sigma_2 (\bar{q}_L \sigma^{\mu\nu} u_R)^T$
	\mathcal{O}_{ledq}	$(\bar{l}_L e_R) (\bar{d}_R q_L)$
	\mathcal{O}_{qe}	$(\bar{q}_L \gamma_\mu q_L) (\bar{e}_R \gamma^\mu e_R)$
	\mathcal{O}_{eu}	$(\bar{e}_R \gamma_\mu e_R) (\bar{u}_R \gamma^\mu u_R)$
	\mathcal{O}_{ed}	$(\bar{e}_R \gamma_\mu e_R) (\bar{d}_R \gamma^\mu d_R)$
QQ	$\mathcal{O}_{qq}^{(1)}$	$(\bar{q}_L \gamma_\mu q_L) (\bar{q}_L \gamma^\mu q_L)$
	$\mathcal{O}_{qq}^{(3)}$	$(\bar{q}_L \gamma_\mu \sigma_a q_L) (\bar{q}_L \gamma^\mu \sigma_a q_L)$
	$\mathcal{O}_{quqd}^{(1)}$	$(\bar{q}_L u_R) (\bar{q}_L d_R)^T$
	$\mathcal{O}_{quqd}^{(8)}$	$(\bar{q}_L T_A u_R) (\bar{q}_L T_A d_R)^T$
	$\mathcal{O}_{qu}^{(1)}$	$(\bar{q}_L \gamma_\mu q_L) (\bar{u}_R \gamma^\mu u_R)$
	$\mathcal{O}_{qu}^{(8)}$	$(\bar{q}_L \gamma_\mu T_A q_L) (\bar{u}_R \gamma^\mu T_A u_R)$
	$\mathcal{O}_{qd}^{(1)}$	$(\bar{q}_L \gamma_\mu q_L) (\bar{d}_R \gamma^\mu d_R)$
	$\mathcal{O}_{qd}^{(8)}$	$(\bar{q}_L \gamma_\mu T_A q_L) (\bar{d}_R \gamma^\mu T_A d_R)$
	\mathcal{O}_{uu}	$(\bar{u}_R \gamma_\mu u_R) (\bar{u}_R \gamma^\mu u_R)$
	$\mathcal{O}_{ud}^{(1)}$	$(\bar{u}_R \gamma_\mu u_R) (\bar{d}_R \gamma^\mu d_R)$
	$\mathcal{O}_{ud}^{(8)}$	$(\bar{u}_R \gamma_\mu T_A u_R) (\bar{d}_R \gamma^\mu T_A d_R)$
	\mathcal{O}_{dd}	$(\bar{d}_R \gamma_\mu d_R) (\bar{d}_R \gamma^\mu d_R)$

Table 1: List of baryon (and lepton) number conserving 4F operators in the Warsaw basis at $d=6$. Note that we have suppressed generation indices here.

In the final step one then needs to identify the quantum numbers for the internal fields of the diagram, given a set of external legs. The procedure is depicted schematically in figure 2 for the example of \mathcal{O}_{ll} . Consider for simplicity first the tree-level: Because \mathcal{O}_{ll} is symmetric in the fields, apart from generation indices, there are only two possible combinations for the outside fields. Both lead to exactly two “models” (due to the $SU(2)$ rule $\mathbf{2} \otimes \mathbf{2} = \mathbf{3} \oplus \mathbf{1}$). Note that the $\mathbf{1}$ is anti-symmetric and thus vanishes for a single generation of leptons.

At one-loop level, there is the complication that at the four corners of the loop diagram one SM field couples to two unknown fields, thus the quantum numbers of the particles in the loop are not unequivocally fixed. We can write the quantum numbers of the scalars

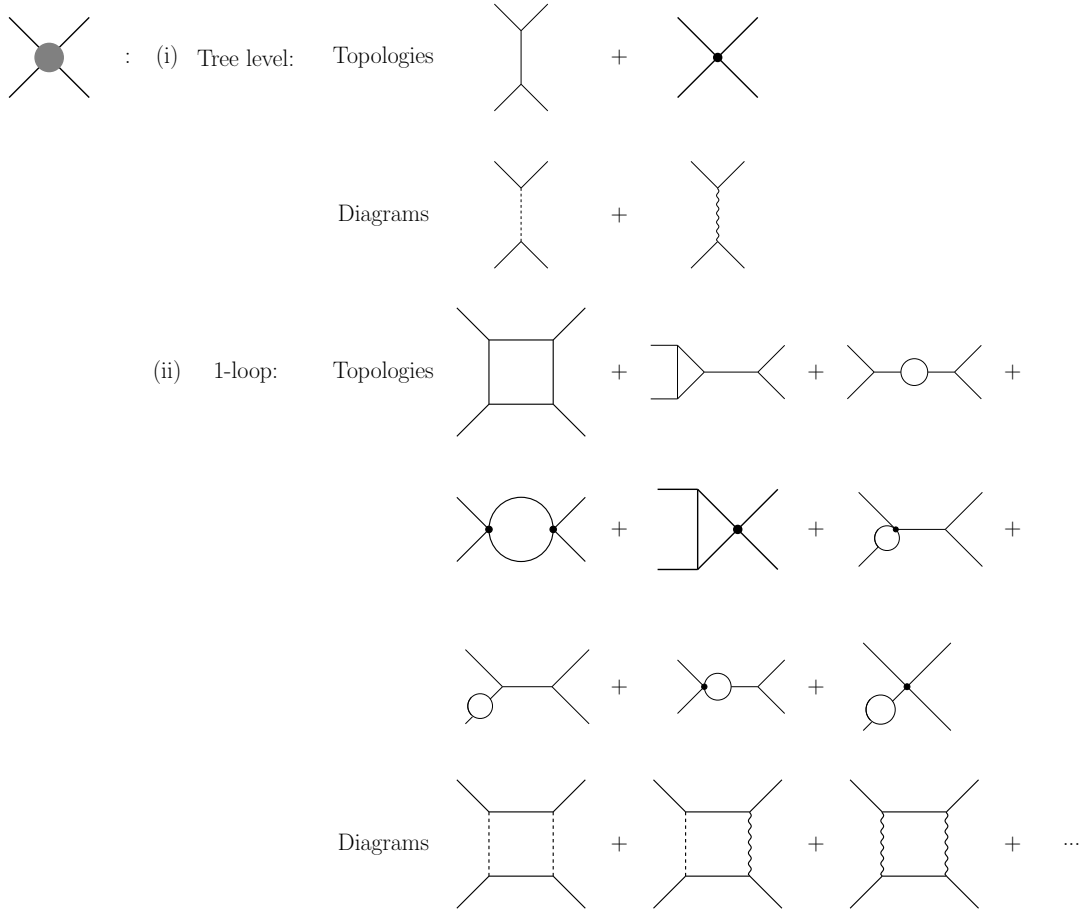


Figure 1: The figure illustrates the first two steps in the diagrammatic method for the construction of UV model lists. 4-point vertices are marked with a dot. For a discussion see text.

and fermions in the diagrams as $S_i(c_S^i, n_S^i, y_S^i)$ and $F_i(c_F^i, n_F^i, y_F^i)$, with $i = 1, 2$ (in some examples only one type of fermion and/or scalar appears) and so on. For this simple 4F operator $c_S^1 = c_F^1$ and $n_F^1 = n_S^1 \pm 1$, while y_S^i and y_F^i are related by $\pm 1/2$. For other operators the relations may be more complicated, but with the help of, for example, **GroupMath** [28] any necessary set of rules can be calculated in an automated way. A list of valid models can then be arrived at by inserting a set of seed fields. The list of seeds needs to fix one of the particles internal to the loop, all other particle quantum numbers can then be calculated. The conditions that we use in the current paper to select the lists of seed fields (and all other cuts on the models) are discussed in subsection 2.2. The method itself, however, is completely agnostic to this choice and works for any list of seeds. Finally, this procedure has to be repeated for all valid permutations of outside fermion fields. The result is a list of adjacency matrices, whose entries are the quantum numbers and Lorentz nature of the

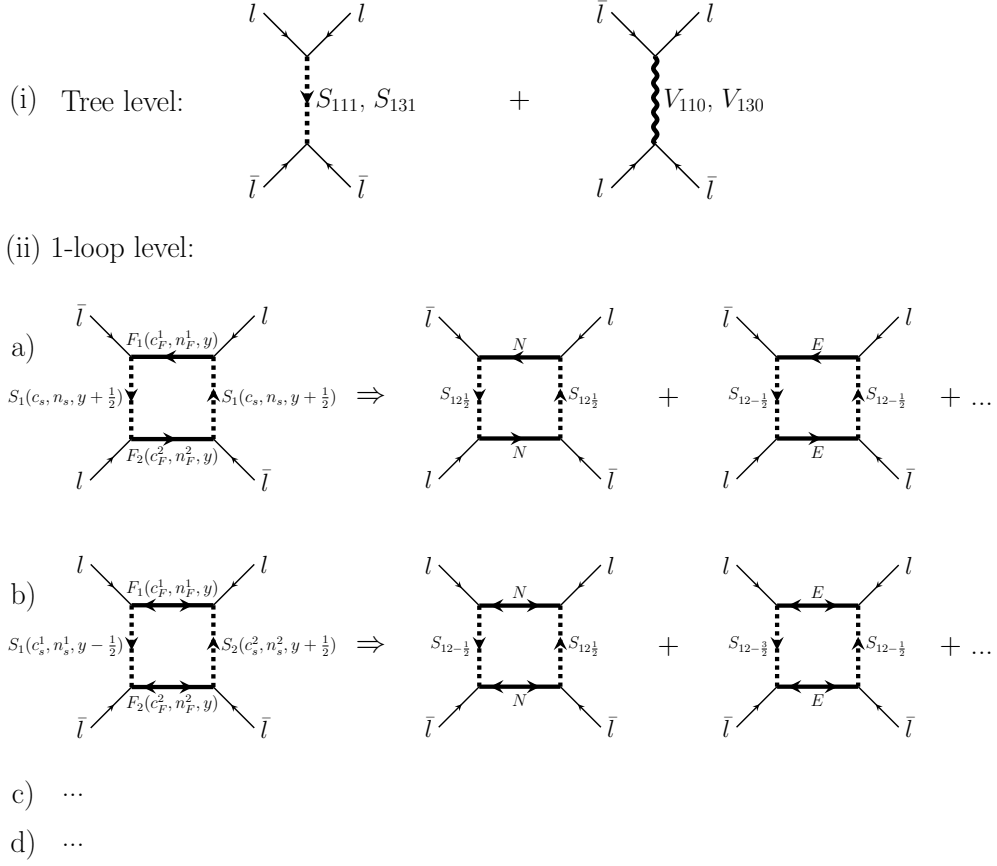


Figure 2: The figure illustrates the construction of UV models for a given diagram with fixed outside legs. For simplicity of presentation we have chosen a symmetric operator, \mathcal{O}_l in this example, since it yields the minimal number of models (four at tree-level). Note that in diagrams with specific particles inserted, we use arrows to track the flow of quantum numbers, such as colour and hypercharge. For vector-like and Majorana fermions, the double arrows indicate a mass insertion.

particles in the diagram. From this list one finally deletes all model duplicates.³

We call diagrams with all particle properties inserted (both Lorentz nature and quantum numbers) “model-diagrams” or models for short. Strictly speaking, the diagrammatic method, as described above, does not give full-fledged models, it only specifies their particle content. However, again existing programs such as **Sym2Int** [29] make it possible to calculate the full Lagrangian of these models with only the particle content as input in an automated way.

³As a technical aside, we add that we keep track of the fermion chiralities in the diagrams too, since this determines the power of loop momenta as well as possible internal SM fields. For example, boxes with an odd power of loop momenta vanish identically for operators without derivatives (such as the 4F under consideration here) and thus such diagrams do not represent valid models for 4F operators.

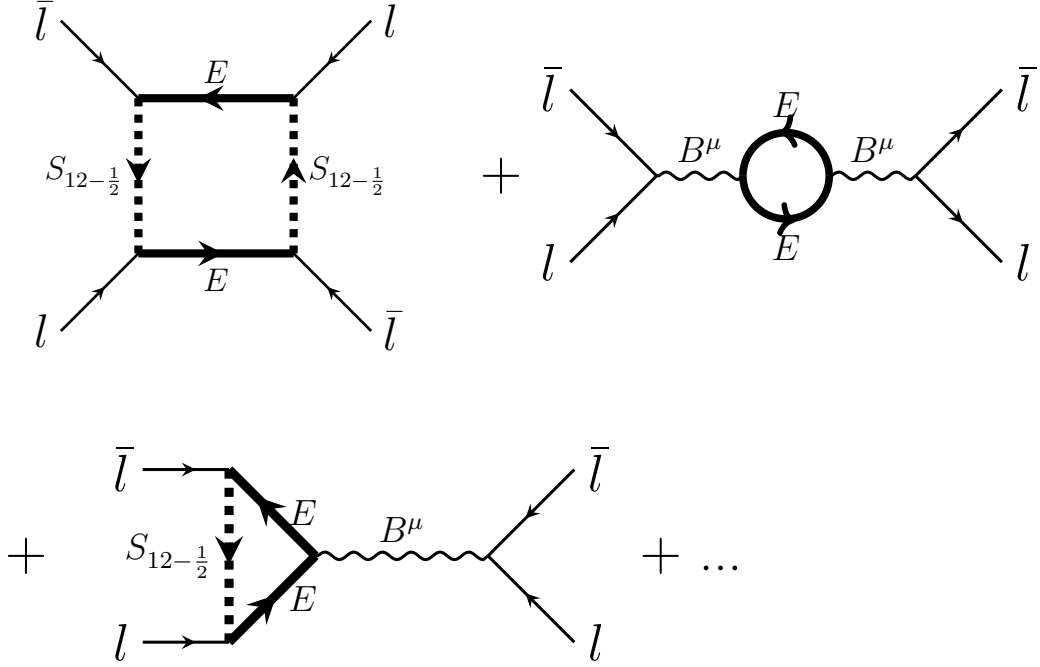


Figure 3: The figure illustrates how light particle reducible diagrams are generated, going from the complete Green’s basis to the on-shell Warsaw basis, see text.

While the diagrammatic method can be used for model constructions for any type of operator, there is a subtlety involved in the matching of models to a particular operator basis. Let us discuss this in some detail. The Warsaw basis for $d = 6$ SMEFT [3] gives the complete on-shell list of operators. It uses all possible relations among operators based on integration-by-parts (IBP), equations of motion (EOM) and Fierz transformations to eliminate redundant operators. While it obviously makes sense physically not to list redundant operators, it is sometimes very useful to consider the over-complete set of operators in the so-called Green’s basis instead.

Consider, for example, $(D_\mu X^{\mu\nu})^2$, where $X^{\mu\nu}$ stands symbolically for any of the three SM fields strength tensors. This operator exists in the Green’s basis, but is eliminated in the Warsaw basis by the equation of motion for the field strength tensor: $\mathcal{O}_{D^2 X^2} \propto (D_\mu X^{\mu\nu}) = \bar{\psi} \gamma^\nu \psi + \phi^\dagger i \overleftrightarrow{D}^\nu \phi$, where ψ includes any SM fermion charged under the group to which $X^{\mu\nu}$ belongs. Any BSM state that is not a complete singlet under the SM group will couple also to gauge bosons. Thus, any non-singlet BSM fermion will appear in $\mathcal{O}_{D^2 X^2}$ at one-loop level with a contribution proportional to g_i^2 , which then gives a contribution to all 4F operators involving ψ coupled to $X^{\mu\nu}$, when going to the on-shell Warsaw basis.

In the diagrammatic method, when fixed to the Warsaw basis, these contributions appear as light-particle reducible diagrams contributing to the operator under consideration, see figure 3. The figure shows for one example model how not only the box diagrams contribute to the operator \mathcal{O}_ll and lists the other diagrams in which $B^{\mu\nu}$ appears. (Again, the list of diagrams shown is not complete. The figure is for illustration only.) Compare to the topologies in the lower half of figure 1. Thus, changing between Green’s and Warsaw basis affects the matching of 4F operators in a non-trivial way and one always needs to specify the basis, in which the matching results are quoted. The construction of model diagrams is simpler in the Green’s basis, since there we do not need to consider light-particle reducible diagrams, while in the Warsaw basis (with fewer operators) such diagrams need to be included for a complete matching since they correspond to applying EOMs to the operators in the Green’s basis.

Note, however, that contributions due to $(D_\mu X^{\mu\nu})^2$ are universal and diagonal in flavour space. Matching 4F operators at one-loop will contain terms proportional to, say, λ^4 , $g_i^2 \lambda^2$, $\lambda^2 \lambda_{SM}^2$ etc., where λ stands symbolically for a BSM Yukawa, λ_{SM} are SM Yukawas and g_i is any of the gauge couplings. Since $\forall \lambda_{SM} \ll 1$ (except for the top quark) and also $g_1, g_2 < 1$ while there is a priori no reason why λ should be small, for a rough estimate it is often sufficient to discuss matching in the limit where all SM couplings are set to zero. Diagrammatically this corresponds to considering only box diagram contributions to the 4F operators. For the example models discussed in more detail in section 3.4, however, we also briefly comment on the complete matching.

The output of our method is a list of model diagrams. For the matching of specific models onto the SMEFT operators we use `MatchmakerEFT` [30]. Note that `MatchmakerEFT` follows a similar logic in the calculation of matching coefficients as discussed here. It calculates matching first in the Green’s basis before converting the output to the Warsaw basis (or any other basis provided by the user).

2.2 Restrictions for LHC-testable UV models

In this subsection, we discuss the three main restrictions which we apply to our list of models. As a short summary up front: (a) Use only models with BSM scalars and fermions, but no new vectors; (b) select only models which do not produce any stable charged relics; and (c) select only models for which no 4F operator appears at tree-level.

Let us discuss vectors first. Ref. [18] gives the complete lists of BSM particles, including also all vectors, which could contribute to $d = 6$ SMEFT at tree-level. However, while it is fairly straightforward to construct all diagrams containing vector particles, consistent model building for *gauge vectors* is highly non-trivial.

There are two unrelated problems for models with gauge vectors. First, gauge vectors are in the adjoint of the gauge group. From the quantum numbers of the vectors one can find the minimal gauge group in which a given vector can be part of the adjoint. This exercise has been done, for example, in [31]. Note that that paper studied neutrinoless double beta decay, but the list of vectors covers all but one of the vectors listed in [18].⁴

⁴[31] contains more vectors than the list in [18], since it discusses double beta decay up to $d = 11$. The

It has been found that for the majority of these vectors, the groups are very exotic and it is not even possible to construct a model which can be broken to the SM gauge group with SM field content in a consistent way [31] if the SM fermions transform non-trivially under the extended gauge group too.

The second problem with vectors is purely phenomenological. For a number of vectors in the list of “exit” vectors one finds that the minimal possible gauge groups are grand unified groups, such as $SU(5)$, flipped $SU(5)$ or also $SO(2n)$ groups. In these cases, proton decay constraints require that the vectors live at the GUT scale, rendering them completely uninteresting for electro-weak scale phenomenology. We note that the recent work [33] circumvents this problem partially by assuming all SM fermions to be singlet under the new gauge group. Interactions with the new gauge bosons are then generated via mixing of the SM fermions with exotic, vector-like copies, where the latter are assumed to transform non-trivially under the new gauge group *and* the SM group. However, while in such a setup the exotic gauge bosons can be lighter than the classical GUT scale in principle, the model construction has to be done in a specific way, such that baryon and lepton numbers are conserved, otherwise the proton decay constraints will apply again. Given these complications, in this paper we will concentrate exclusively on models with only scalar and fermion BSM fields.

The second restriction we use to select models is purely phenomenological. Consider the following: At one-loop level vertices will appear in which the BSM fields couple in pairs to a single SM particle. The simplest possible example is a gauge boson coupling to a pair of fermions $\psi - \bar{\psi}$. Since one can always find a singlet in $\psi - \bar{\psi}$, it seems one could build an *infinite tower of one-loop models*, simply by going to larger representations and/or larger hypercharges. However, in practice, there are restrictions for model building, which will provide a cutoff in this a priori infinite series.

For model constructions which aim at generating interesting LHC phenomenology, the most important restriction is that experimental searches for stable charged relics essentially exclude the mass range $M \sim [1, 10^5]$ GeV, see for example [34–37]. Thus no model containing a stable, charged BSM field can give any LHC phenomenology. To avoid this constraint we have to assume either (a) the BSM fields are unstable or (b) the lightest of the BSM fields is a good dark matter candidate. These two possibilities will lead to very different phenomenology at the LHC, if the BSM particles are light enough to be produced on-shell. Here, we will concentrate on models in class (a). However, we plan to return to the dark matter option in a future publication.

Consider class (a). In the following, we will call certain BSM fields “exit particles”, or exits for short. An exit is defined as any BSM particle that can appear linearly in a Lagrangian term with SM fields. Such particles then are guaranteed to be unstable. They are therefore synonymous with the list of particles that can generate the $d = 6$ SMEFT operators at tree-level. The complete lists of these exits can be found in [18]. As already mentioned in the introduction, this list is finite. Thus, at one-loop level also the number of

one missing vector, on the other hand, is $\mathcal{U}_5 = V_{3,1,5/3}$. This vector appeared, for example, in [32], where it was found that it could be generated from the Pati-Salam group, albeit in a non-standard embedding.

Name	\mathcal{S}	Ξ	Θ_1	Θ_3
Irrep	$(1, 1, 0)$	$(1, 3, 0)$	$(1, 4, \frac{1}{2})$	$(1, 4, \frac{3}{2})$

Table 2: Scalar “exits” that do not generate tree-level four-fermion operators. Symbols use the notation of [18]. The numbers in brackets refer to the representations of the SM gauge groups $SU(3)_C$, $SU(2)_L$ and $U(1)_Y$.

models pertaining to this class is finite.

Before turning to our third restriction on model building, we mention in passing that also other arguments providing a cutoff for the “infinite” series of one-loop models exist. For example, one may want to argue that any interesting BSM extension should maintain the perturbativity of the gauge couplings up to some large energy scale, say for example the grand unification scale, m_G or even the Planck scale. See for example [38] for a recent discussion on how this argument limits the number of viable models in the case of the Weinberg operator. In this paper, we do not use such theoretical arguments.

Finally, we will further limit our list of models by excluding all models of a one-loop generated 4F operator whose particle content produces any other 4F operator at tree-level. Again, this restriction is simply driven by our desire to find models that can be studied at the LHC. Tree-level generated $d = 6$ operators will lead to restrictions on the new physics scale Λ which are typically stronger by a factor of 4π than the ones found for one-loop generated operators as discussed above, see also Fig. 4.

In terms of model generation, the practical consequence of this choice is that not all possible scalar exits can appear in our model list. In Table 2 we list the four scalar exits in this class. \mathcal{S} and Ξ will decay to two Higgses (or, of course, gauge bosons, after electro-weak symmetry breaking), while $\Theta_{1,3}$ decay to three Higgses. Table 3 gives the list of fermion exits for completeness. None of the fermions can produce a 4F operator at tree-level, thus this list is identical to the one found in [18].

One last, purely phenomenological, restriction we use to limit the number of generated models consists in neglecting all models that produce only diagrams that are proportional to at least some SM Yukawa (λ_{SM}) or gauge (g_i) couplings, for example $\lambda_{SM}^2 \lambda^2$. The reason for not considering such models is that, except for the top quark, $\lambda_{SM} \ll 1$ and consequently a diagram involving an SM Yukawa coupling will be suppressed with respect to any diagram that contains only BSM couplings that we assume to be naturally of order $\mathcal{O}(1)$. However, as noted above, in the actual matching process done by `MatchmakerEFT` all SM Yukawa couplings will be taken into account, leading to “exact” matching results.

2.3 Tree-level $\psi^2 H^2 D$ and $\psi^2 H^3$ operators

As discussed above, in this paper we study models that generate 4F operators only at the one-loop level. However, choosing models which contain one of the exit particles of Tables 2 and 3, some operators from two other classes, $\psi^2 H^2 D$ and $\psi^2 H^3$, will be generated at tree-level. Table 4 shows all operators involving two fermions and two Higgs bosons and

Name	N	E	Δ_1	Δ_3	Σ	Σ_1
Irrep	$(1, 1, 0)$	$(1, 1, -1)$	$(1, 2, -\frac{1}{2})$	$(1, 2, -\frac{3}{2})$	$(1, 3, 0)$	$(1, 3, -1)$

Name	U	D	Q_1	Q_5	Q_7	T_1	T_2
Irrep	$(3, 1, \frac{2}{3})$	$(3, 1, -\frac{1}{3})$	$(3, 2, \frac{1}{6})$	$(3, 2, -\frac{5}{6})$	$(3, 2, \frac{7}{6})$	$(3, 3, -\frac{1}{3})$	$(3, 3, \frac{2}{3})$

Table 3: Fermion exits: New vector-like fermions that can couple linearly to standard model particles. Symbols are taken from [18].

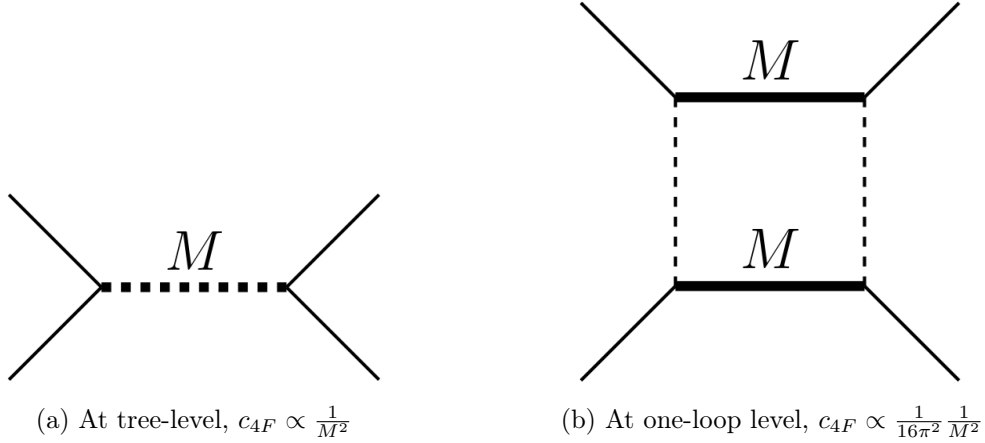


Figure 4: Sample diagrams at tree-level and one-loop level. The one-loop contribution to the Wilson coefficient is suppressed by a factor of $16\pi^2$ with respect to the tree-level contribution.

one derivative or three Higgs bosons. Anyway, for our models not all of these operators are generated by each model. Which of these operators is generated depends on the exit particle of the model under consideration.

3 Model candidates and their matching to 4F operators

In this section we will count the number of UV completions leading to loop-suppressed 4F operators, describe their matter content and discuss some common aspects they share.

3.1 Counting UV completions

The Warsaw basis counts 25 baryon number conserving 4F operator structures at dimension-6, cf. Table 1, suppressing flavour indices. Note that while the model diagrams can be understood as having open flavour indices, in practice we will be interested only in flavour diagonal operators. The reason for this restriction is that for flavour-violating operators experimental constraints are usually much stronger than for flavour conserving ones, in particular if the operators contain leptons [17].

class	name	structure
$\psi^2\phi^2D$	$\mathcal{O}_{\phi l}^{(1)}$	$\left(\phi^\dagger i\overleftrightarrow{D}_\mu\phi\right) (\bar{l}_L\gamma^\mu l_L)$
	$\mathcal{O}_{\phi l}^{(3)}$	$\left(\phi^\dagger i\overleftrightarrow{D}_\mu^a\phi\right) (\bar{l}_L\gamma^\mu\sigma^a l_L)$
	$\mathcal{O}_{\phi e}$	$\left(\phi^\dagger i\overleftrightarrow{D}_\mu\phi\right) (\bar{e}_R\gamma^\mu e_R)$
	$\mathcal{O}_{\phi q}^{(1)}$	$\left(\phi^\dagger i\overleftrightarrow{D}_\mu\phi\right) (\bar{q}_L\gamma^\mu q_L)$
	$\mathcal{O}_{\phi q}^{(3)}$	$\left(\phi^\dagger i\overleftrightarrow{D}_\mu^a\phi\right) (\bar{q}_L\gamma^\mu\sigma^a q_L)$
	$\mathcal{O}_{\phi u}$	$\left(\phi^\dagger i\overleftrightarrow{D}_\mu\phi\right) (\bar{u}_R\gamma^\mu u_R)$
	$\mathcal{O}_{\phi d}$	$\left(\phi^\dagger i\overleftrightarrow{D}_\mu\phi\right) (\bar{d}_R\gamma^\mu d_R)$
	$\mathcal{O}_{\phi ud}$	$\left(\phi^\dagger i\overleftrightarrow{D}_\mu\phi\right) (\bar{u}_R\gamma^\mu d_R)$
$\psi^2\phi^3$	$\mathcal{O}_{e\phi}$	$(\phi^\dagger\phi)^2 (\bar{l}_L\phi e_R)$
	$\mathcal{O}_{u\phi}$	$(\phi^\dagger\phi)^2 (\bar{q}_L\phi u_R)$
	$\mathcal{O}_{d\phi}$	$(\phi^\dagger\phi)^2 (\bar{q}_L\phi d_R)$

Table 4: Fermion-Higgs operators at dimension-6 in the Warsaw basis.

In the following counting, for simplicity, we will not distinguish between singlet and non-singlet operators with the same fermion content, for example we simply write \mathcal{O}_{lq} for $\mathcal{O}_{lq}^{(1)}$ and $\mathcal{O}_{lq}^{(3)}$. Thus, the basis simplifies to 18 B-conserving 4F operators which can be classified into 3 categories:

1. 3 lepton-specific operators (in the following referred to as LL): \mathcal{O}_{ll} , \mathcal{O}_{le} and \mathcal{O}_{ee}
2. 7 quark-specific operators (QQ): \mathcal{O}_{qq} , \mathcal{O}_{quqd} , \mathcal{O}_{qu} , \mathcal{O}_{qd} , \mathcal{O}_{uu} , \mathcal{O}_{ud} , \mathcal{O}_{dd}
3. 8 mixed lepton-quark operators (LQ): \mathcal{O}_{lq} , \mathcal{O}_{lu} , \mathcal{O}_{ld} , \mathcal{O}_{lequ} , \mathcal{O}_{leqd} , \mathcal{O}_{qe} , \mathcal{O}_{eu} , \mathcal{O}_{ed}

The diagrammatic method, discussed in the previous section, has been implemented into a Mathematica code, which we call the *ModelGenerator*. Using the *ModelGenerator* we have found all UV models that open up any of these 18 operator structures at one-loop and meet the criteria discussed in section 2.2.

Moreover, we still have the freedom to define a maximal size of the representation we want to allow the UV model particles to have under the SM gauge groups, i.e. we can specify maximal values for $SU(3)_C$, $SU(2)_L$ and the hypercharge Y. We call these $maxSU3$, $maxSU2$ and $maxY$ in the following. Considering all of the exit particles in Tables 2 and 3, it is easy to determine that the maximal possible representation sizes (and numbers) in our models are $maxSU3 = 8$, $maxSU2 = 6$, $maxY = 5$.

Once we found the models for all the 18 operators, and before we study some models in detail, it is interesting to cast a glance on the interplay between the operators and to

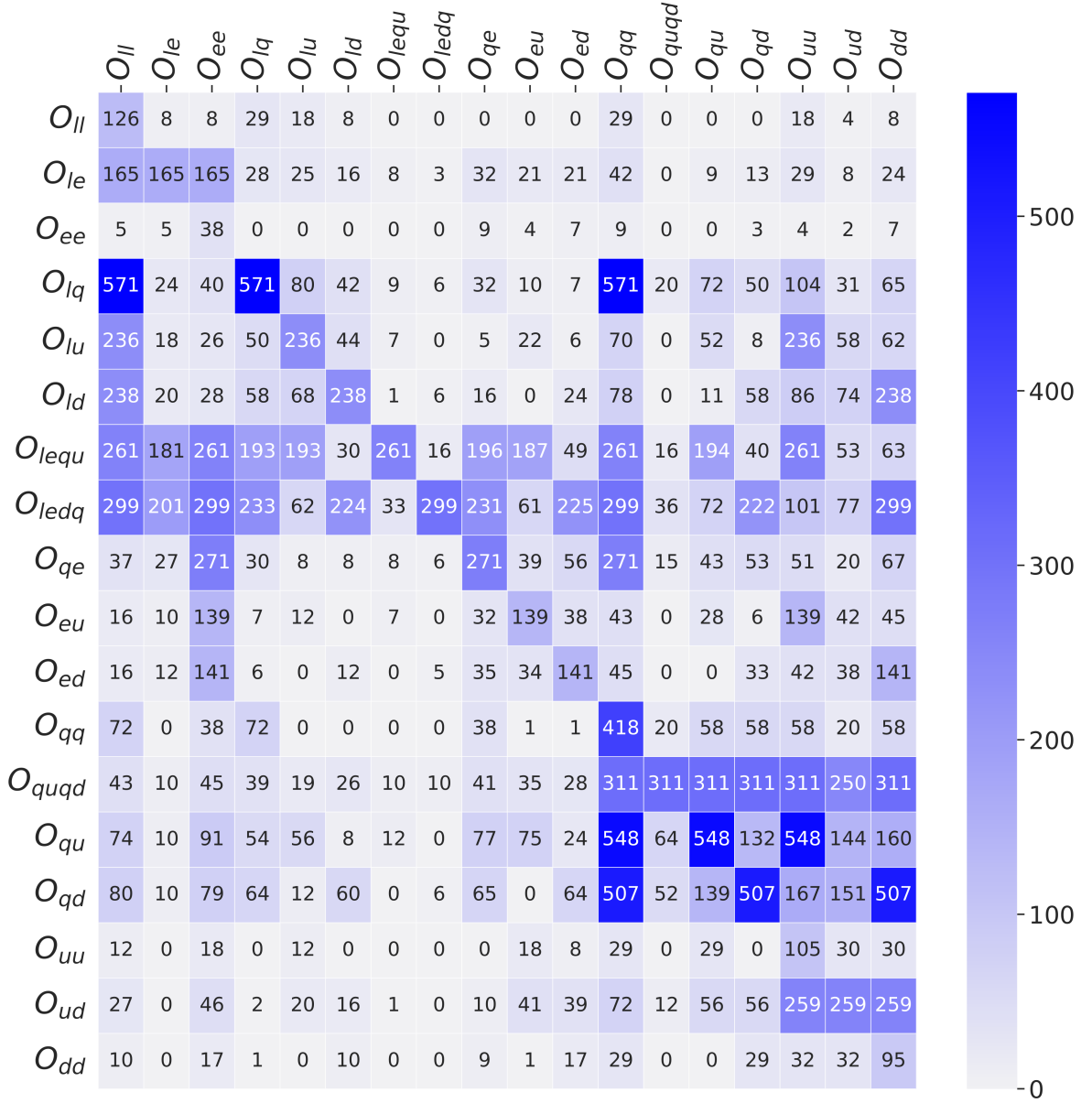


Figure 5: Operator overlap matrix for $\max SU3 = 8$, $\max SU2 = 6$ and $\max Y = 5$. The table counts the number of models for each operator in the diagonal, the off-diagonal counts the “model overlap”, see text.

analyse which models found for one operator can also open up one of the other operators at one-loop level. Depending on the structure of the operator, a model can contain between two and four different BSM particles. So picking one model and rearranging the particles in the loop or picking a subset of the particles and repeating some of them can lead to a box-diagram for another 4-fermion operator.

In Fig. 5 we list the number of models found for one operator that can open up any

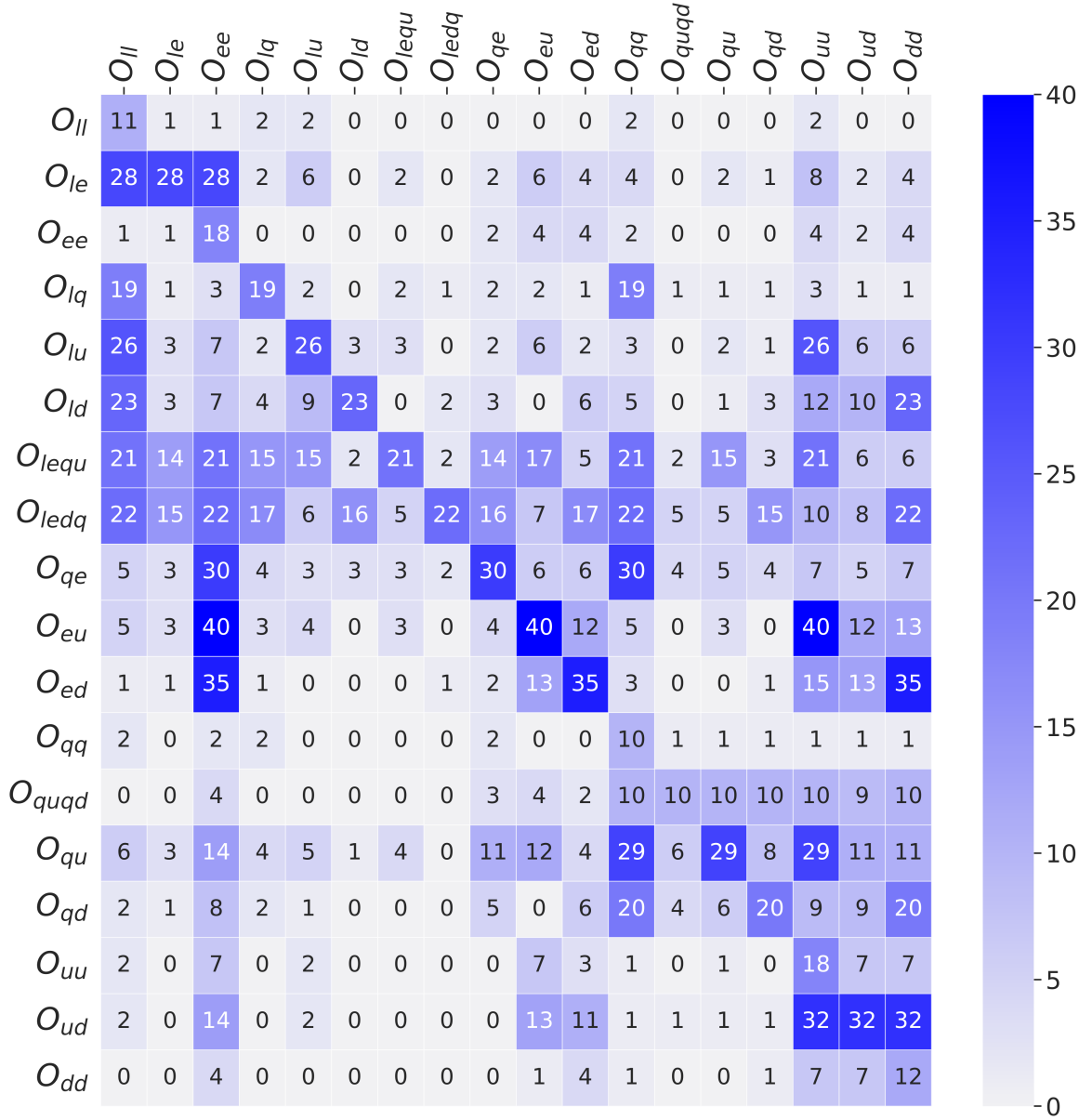


Figure 6: Operator overlap for $maxSU3 = 3$, $maxSU2 = 2$ and $maxY = 4$.

of the other 17 4-fermions operators for the maximal possible representation $maxSU3 = 8$, $maxSU2 = 6$ and $maxY = 5$. To emphasise the large hierarchy between the entries in the matrix, we underlie the table with a heat-map, with darker colours representing larger numbers.

The table is to be read in the following way: The diagonal entries list the total number of models for this operator. Every row belongs to one operator, say \mathcal{O}_X . Then, every entry in this row lists how many of the models for operator \mathcal{O}_X provide a contribution to the operator that labels the column.

To give an explicit example: the third row states that we found 38 models for the operator \mathcal{O}_{ee} out of which 5 open up \mathcal{O}_{ll} , 5 \mathcal{O}_{le} , 9 \mathcal{O}_{qe} , 4 \mathcal{O}_{eu} , 7 \mathcal{O}_{ed} , 9 \mathcal{O}_{qq} , 3 \mathcal{O}_{qd} , 4 \mathcal{O}_{uu} , 2 \mathcal{O}_{ud} and 7 \mathcal{O}_{dd} . All the other entries in this row being zero means that none of the models for \mathcal{O}_{ee} can be recasted in a box that contributes to \mathcal{O}_{lq} , \mathcal{O}_{lu} , \mathcal{O}_{ld} , \mathcal{O}_{lequ} , \mathcal{O}_{ledq} , \mathcal{O}_{quqd} or \mathcal{O}_{qu} .

As one can see from Fig. 5, the number of possible models is still large (571 models for \mathcal{O}_{lq} , for example). Since it is nearly impossible to study the phenomenology for all of these, it is useful to reduce the number of models by limiting the maximal allowed representations. The exact choice for $maxSU3$, $maxSU2$ and $maxY$ is of course somewhat arbitrary. However, since this choice is a simple post-selection on a larger existing model list, such cuts can be done straight-forwardly for any choice of $maxSU3$, $maxSU2$ and $maxY$ one may wish to consider. In Fig. 6 we show the overlap matrix for the concrete choice of $maxSU3 = 3$, $maxSU2 = 2$ and $maxY = 4$. The matrix is obviously much sparser. For example, for \mathcal{O}_{lq} only 19 models remain. Most interesting, however, is that in this table many more zeroes appear. Thus, it would become much easier to gain information on the underlying UV model if some non-zero coefficients for the 4F operators had been established experimentally.

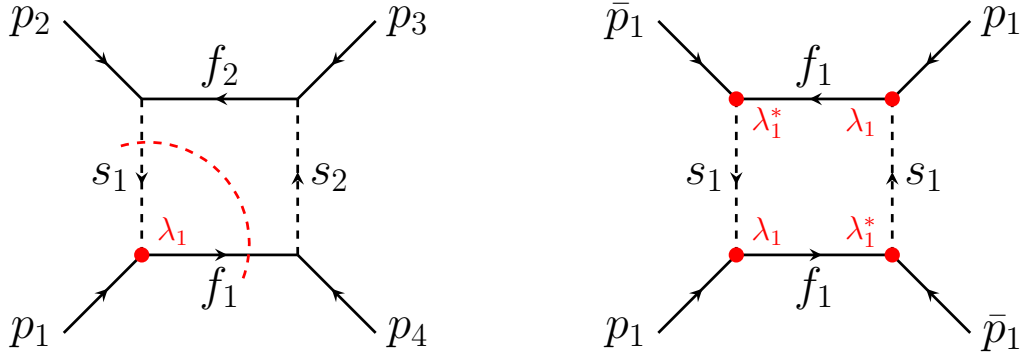
In the following subsections we will discuss some benchmark models for the three different operator classes, LL, LQ and QQ.

3.2 Patterns in SMEFT 4F operators

The inspection of Fig. 5 and 6 shows that there is still a large number of possible models even after imposing all the simplifying assumptions we described in subsection 2.2. However, the model overlap matrix becomes quite sparse, especially when focusing on lower representations of the SM gauge groups, Fig. 6.

Also, it is clear that the tables are not symmetric due to the structure of the different operators. This means that if we have n models for operator \mathcal{O}_2 that open up operator \mathcal{O}_1 , it does not necessarily imply that any of the models for operator \mathcal{O}_1 also opens up \mathcal{O}_2 . For example, consider an operator \mathcal{O}_1 generated by some model with only two different particles, F_1 and S_1 , such that the box opening reads as $\mathcal{M}_1 = \{F_1, S_1, F_1, S_1\}$. Then, for any viable combination of particles F_2 and S_2 , the model $\mathcal{M}_2 = \{F_1, S_1, F_2, S_2\}$ will generate operator \mathcal{O}_2 , as well as \mathcal{O}_1 via the same model \mathcal{M}_1 , which is a subset of \mathcal{M}_2 . But, as long as no opening of \mathcal{O}_1 features the particles F_2 and S_2 , no model for \mathcal{O}_1 will open up \mathcal{O}_2 .

To see an explicit example, consider \mathcal{O}_{le} and \mathcal{O}_{ll} : For $maxSU3 = 3$, $maxSU2 = 2$ and $maxY = 4$ all 28 models for \mathcal{O}_{le} also open up \mathcal{O}_{ll} , but only one out of 11 models for \mathcal{O}_{ll} opens \mathcal{O}_{le} . As mentioned before, this is the case because all model-diagrams for \mathcal{O}_{le} generate also \mathcal{O}_{ll} . A schematic example of how this works is shown in figure 7: Identifying p_1 with the lepton doublet l and being (p_2, p_3, p_4) any permutation of $(\bar{l}, e_R, \bar{e}_R)$, the left side presents a box diagram for \mathcal{O}_{le} . Introducing the coupling λ_1 between p_1 , s_1 and \bar{f}_1 , we note that cutting the lower left corner and stitching it together with itself and two copies of its complex conjugate leads to a diagram for \mathcal{O}_{ll} , as it is shown on the right side of Fig. 7.



(a) Generic 4F operator with up to four different external legs.

(b) Generic 4F operator with all four legs being the same SM particle.

Figure 7: Schematic example how to obtain models for *more symmetric* 4F operators from models for *less symmetric* ones. A model that generates an operator of the form $\mathcal{O}_{p_1 p_2 p_3 p_4}$ will automatically produce also the operators $\mathcal{O}_{p_1 p_1}$, $\mathcal{O}_{p_2 p_2}$, $\mathcal{O}_{p_3 p_3}$ and $\mathcal{O}_{p_4 p_4}$. See text for details.

On the other hand, finding a model that generates \mathcal{O}_{le} from the list of models that opens \mathcal{O}_l is not straightforward. Due to the symmetry of the external particles of \mathcal{O}_l , in general less fields are needed to generate this operator and, thus, one would have to add more particles to obtain a model for \mathcal{O}_{le} . The one model for \mathcal{O}_l that opens up \mathcal{O}_{le} features only the particles S and Δ_1 : $(S, \Delta_1, S, \bar{\Delta}_1)$. This is a rather particular case where the SM Higgs, along with S and Δ_1 , participates in the box diagram that generates \mathcal{O}_{le} .

This analysis allows us to start identifying common patterns among models. First, many of these scenarios exclusively produce LL or QQ types of operators. Second, all of the models which produce LQ operators also produce LL and QQ operators. The argument for this is very similar to the one provided above for \mathcal{O}_{le} and \mathcal{O}_l : Consider an operator $\mathcal{O}_{p_1 p_2 p_3 p_4}$ of the class LQ, i.e. two p's are quarks and two of them are leptons. Then, every model for $\mathcal{O}_{p_1 p_2 p_3 p_4}$ will produce $\mathcal{O}_{p_1 p_1}$, $\mathcal{O}_{p_2 p_2}$, $\mathcal{O}_{p_3 p_3}$ and $\mathcal{O}_{p_4 p_4}$ by taking a subset of the two internal particles of the original model which are adjacent to the respective p_i , exactly as it has been explained for \mathcal{O}_{le} and \mathcal{O}_l , see Fig. 7 again.

This means that, for instance, all models for \mathcal{O}_{eq} will produce both \mathcal{O}_{ee} and \mathcal{O}_{qq} , while for example the models for \mathcal{O}_{ledq} will contribute to all of the four operators \mathcal{O}_l , \mathcal{O}_{ee} , \mathcal{O}_{qq} and \mathcal{O}_{dd} .

Based on these observations, we can classify three types of scenarios:

- **Lepton-specific scenarios:** exclusively producing 4F involving leptons.
- **Quark-specific scenarios:** constrained to affecting hadronic observables.
- **Generic or hybrid scenarios:** which contribute to the three types of 4F operators.

Within each of these categories, we find models with different matter content. A further simplifying criterion one imposes is *minimality*, i.e. to identify which specific models contain

the least number of new particles and hence of new parameters. In subsection 3.5 we will discuss the quark-specific models in a bit more detail.

3.3 New particles running in loop-induced 4F operators

We now examine the actual matter content in these models. As expected, new types of particles will appear in the UV completions and will be shared among models. In particular, if we restrict ourselves to a maximum representation of triplets for $SU(3)_c$ and doublets for $SU(2)_L$, the list of new quantum numbers which show up in the UV completions is not long. We show those new particle candidates in Tables 5 and 6, which we label following the pattern used in the Granada convention [18].

Name	Q_{11}	Q_{13}	Q_{17}	X_4	X_5	X_7	Δ_5	N_2
Irrep	$(3, 2, -\frac{11}{6})$	$(3, 2, \frac{13}{6})$	$(3, 2, -\frac{17}{6})$	$(3, 1, -\frac{4}{3})$	$(3, 1, \frac{5}{3})$	$(3, 1, -\frac{7}{3})$	$(1, 2, \frac{5}{2})$	$(1, 1, 2)$

Table 5: New vector-like fermions.

New fermions Q_a and X_a , similar to quarks Q_L and u_R and d_R , but with unusual hypercharges, appear in many realisations. New colour singlets Δ_5 and N_2 , similar to the leptons in the SM, also appear with non-standard hypercharges as well.

Name	Π_5	Π_{11}	Π_{13}	ω_5	ϕ_3
Irrep	$(3, 2, -\frac{5}{6})$	$(3, 2, -\frac{11}{6})$	$(3, 2, \frac{13}{6})$	$(3, 1, \frac{5}{3})$	$(1, 2, \frac{3}{2})$

Table 6: New scalars.

We also find new coloured scalars Π_a and ω_5 , similar to squarks in supersymmetry, but again with different hypercharge assignments. Finally, a Higgs-like new particle ϕ_3 with hypercharge 3/2 also shows up in some of the UV completions.

In the next section 4, we will discuss the phenomenology of these exotic new particles. Here, we only list the possible “decay channels” for these particles, dictated by our model constructions. Tables 7 and 8 list the decay channels for the allowed exit particles in the models. Note that the “decay channels” shown in these tables are shown before electroweak symmetry breaking. The real, observable decays therefore involve Higgses (h^0) or electroweak gauge bosons (W^\pm or Z^0).

The “decay channels” (before EWSB) of the non-exit particles can be found in Table 9 for scalars and Table 10 for fermions. To determine their decay patterns we used the couplings that necessarily exist for the box diagrams of the models. Note that the non-exit particles could, in principle, be lighter than the exit particle list in this table. In this case, it should be implicitly understood that the exit particle is off-shell and the complete decay chain reads, for example: $\Pi_5 \rightarrow E^* + q \rightarrow q + l + H^\dagger$ and similar for all other cases.

name	representation	decays
\mathcal{S}	$(1, 1, 0)$	$S \rightarrow H + H^\dagger$
Ξ	$(1, 3, 0)$	$\Xi \rightarrow H + H^\dagger$
Θ_1	$(1, 4, \frac{1}{2})$	$\Theta_1 \rightarrow H + H + H^\dagger$
Θ_3	$(1, 4, \frac{3}{2})$	$\Theta_3 \rightarrow H + H + H$

Table 7: Decay channels for scalar exits.

name	representation	decays
N	$(1, 1, 0)$	$N \rightarrow l + H$
E	$(1, 1, -1)$	$E \rightarrow l + H^\dagger$
Δ_1	$(1, 2, -\frac{1}{2})$	$\Delta_1 \rightarrow e_R + H$
Δ_3	$(1, 2, -\frac{3}{2})$	$\Delta_3 \rightarrow e_R + H^\dagger$
Σ	$(1, 3, 0)$	$\Sigma \rightarrow l + H$
Σ_1	$(1, 3, -1)$	$\Sigma_1 \rightarrow l + H^\dagger$
U	$(3, 1, \frac{2}{3})$	$U \rightarrow q + H$
D	$(3, 1, -\frac{1}{3})$	$D \rightarrow q + H^\dagger$
Q_1	$(3, 2, \frac{1}{6})$	$Q_1 \rightarrow u_R + H^\dagger,$ $Q_1 \rightarrow d_R + H$
Q_5	$(3, 2, -\frac{5}{6})$	$Q_5 \rightarrow d_R + H^\dagger$
Q_7	$(3, 2, \frac{7}{6})$	$Q_7 \rightarrow u_R + H$
T_1	$(3, 3, -\frac{1}{3})$	$T_1 \rightarrow q + H$
T_3	$(3, 3, \frac{2}{3})$	$T_3 \rightarrow q + H^\dagger$

Table 8: Decay channels for fermion exits.

3.4 Minimal scenarios and their explicit matching

After identifying the rich set of new states with exotic quantum numbers we find in these scenarios, we move to consider minimal extensions to the SM, i.e. models that include as few non-SM particles as possible.

For lepton- and quark-specific scenarios we can find extensions with only one BSM fermion and a SM Higgs boson, whereas for a hybrid model producing LL, QQ and LQ operators at the same time, it is easy to see that we need two different BSM fermions.

The operators \mathcal{O}_l and \mathcal{O}_{qq} can be opened up by models that contain only one BSM fermion, for example: $E = (1, 1, -1)$ for \mathcal{O}_l and $U = (3, 1, \frac{2}{3})$ for \mathcal{O}_{qq} . The box diagrams are then completed by the SM Higgs boson. Models for the operator \mathcal{O}_{lq} require two different BSM fermions, e.g. E and U . The particle content for each operator is listed in Table 11.

Accordingly, we will consider the Lagrangian $\mathcal{L}_{UV} = \mathcal{L}_{SM} + \mathcal{L}_{NP}$ with \mathcal{L}_{SM} , the unbroken SM Lagrangian and the new particle contribution

$$\mathcal{L}_{NP} = -\lambda_E \bar{E} L H^\dagger - \lambda_U \bar{U} Q H + \text{h.c.} - m_E \bar{E} E - m_U \bar{U} U. \quad (3.1)$$

We stress here that all exotic fermions are considered to be vector-like, i.e. \bar{E} is a different Weyl state and not simply the conjugated state of E .

name	representation	decays
Π_5	$(3, 2, -\frac{5}{6})$	$\Pi_5 \rightarrow E + q$ $\Pi_5 \rightarrow \bar{U} + \bar{q}$ $\Pi_5 \rightarrow \Delta_1 + d_R$ $\Pi_5 \rightarrow \Delta_3 + u_R$ $\Pi_5 \rightarrow \bar{Q}_1 + \bar{u}_R$ $\Pi_5 \rightarrow \bar{Q}_7 + \bar{d}_R$
Π_{11}	$(3, 2, -\frac{11}{6})$	$\Pi_{11} \rightarrow \Delta_3 + d_R$ $\Pi_{11} \rightarrow \bar{Q}_7 + \bar{u}_R$
Π_{13}	$(3, 2, \frac{13}{6})$	$\Pi_{13} \rightarrow \bar{\Delta}_3 + u_R$
ω_5	$(3, 1, \frac{5}{3})$	$\omega_5 \rightarrow \bar{E} + u_R$ $\omega_5 \rightarrow \bar{\Delta}_3 + q$
ϕ_3	$(1, 2, \frac{3}{2})$	$\phi_3 \rightarrow \bar{Q}_5 + u_R$ $\phi_3 \rightarrow Q_7 + \bar{d}_R$

Table 9: Decay channels for non-exit scalar loop particles.

name	representation	decays
Q_{11}	$(3, 2, -\frac{11}{6})$	$Q_{11} \rightarrow \phi_3^\dagger + d_R$ $Q_{11} \rightarrow \omega_5^\dagger + \bar{q}$ $Q_{11} \rightarrow \Pi_{13}^\dagger + \bar{d}_R$
Q_{13}	$(3, 2, \frac{13}{6})$	$Q_{13} \rightarrow \phi_3 + u_R$ $Q_{13} \rightarrow \Pi_{11}^\dagger + \bar{d}_R$
Q_{17}	$(3, 2, -\frac{17}{6})$	$Q_{17} \rightarrow \Pi_{13}^\dagger + \bar{u}_R$
X_4	$(3, 1, -\frac{4}{3})$	$X_4 \rightarrow \phi_3^\dagger + q$ $X_4 \rightarrow \omega_5^\dagger + \bar{d}_R$
X_5	$(3, 1, \frac{5}{3})$	$X_5 \rightarrow \phi_3 + q$ $X_5 \rightarrow \Pi_{11}^\dagger + \bar{q}$
X_7	$(3, 1, -\frac{7}{3})$	$X_7 \rightarrow \omega_5^\dagger + \bar{u}_R$ $X_7 \rightarrow \Pi_{13}^\dagger + \bar{q}$
Δ_5	$(1, 2, \frac{5}{2})$	$\Delta_5 \rightarrow \Pi_{11}^\dagger + u_R$ $\Delta_5 \rightarrow \Pi_{13} + \bar{d}_R$
N_2	$(1, 1, 2)$	$N_2 \rightarrow \omega_5 + \bar{d}_R$ $N_2 \rightarrow \Pi_{11}^\dagger + q$ $N_2 \rightarrow \Pi_{13} + \bar{q}$

Table 10: Decay channels for non-exit fermion loop particles.

This matter content with the new couplings can be found in different scenarios considered in the literature [39, 40]. The particle E is a right-handed massive lepton which mixes with the SM leptons after EWSB and, similarly, U is an up-type right-handed quark mixing with the SM quark. We will assume one generation of each of these states, but more

operator	particles
\mathcal{O}_{ll}	H, E
\mathcal{O}_{qq}	H, U
\mathcal{O}_{lq}	H, E, U

Table 11: Particle content for minimal models for \mathcal{O}_{ll} , \mathcal{O}_{lq} and \mathcal{O}_{qq} .

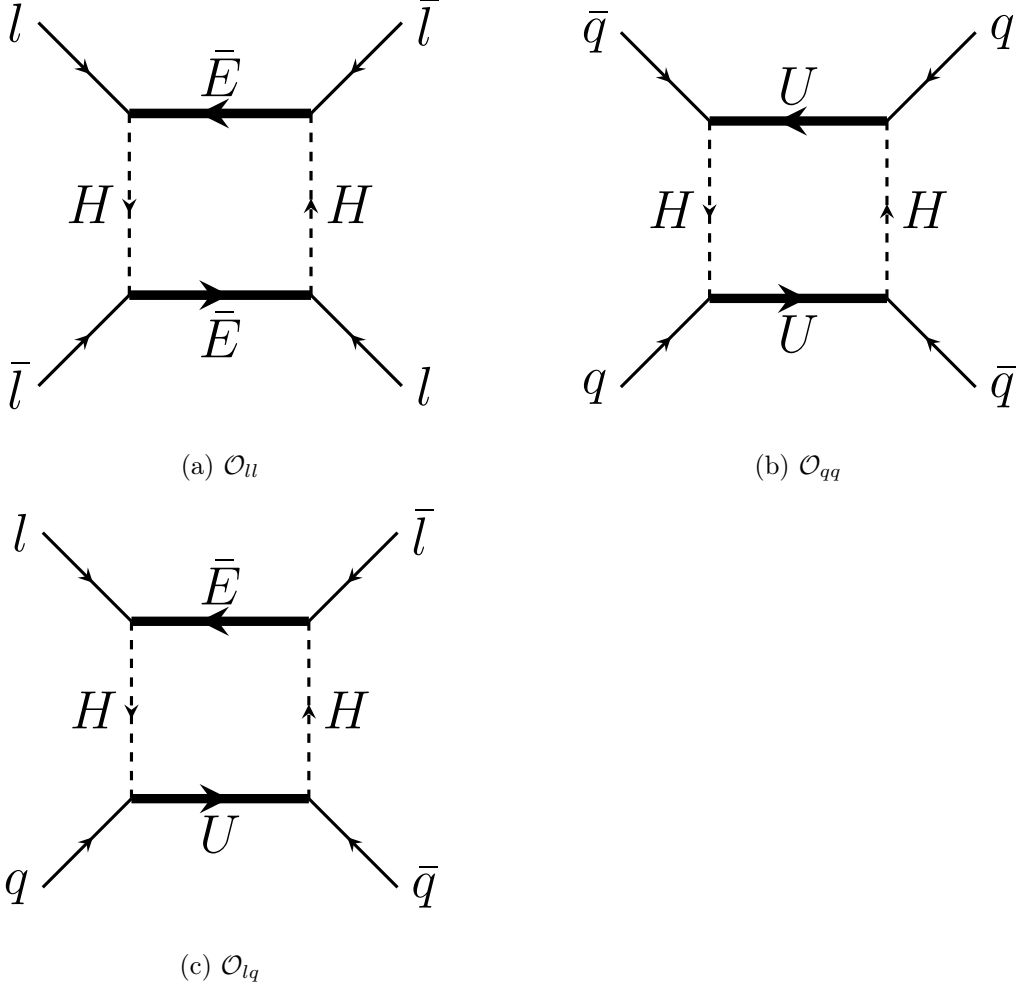


Figure 8: Minimal models for the operators \mathcal{O}_{ll} , \mathcal{O}_{qq} and \mathcal{O}_{lq} .

general scenarios could lead to interesting flavour signatures.

Given this Lagrangian, we can calculate the matching to the SMEFT with the dimension-6 operators in the Warsaw basis, cf. Table 1 by evaluating loop contributions as shown in Fig. 8. We performed the exact matching with `MatchmakerEFT` [30].

The matching of the simple benchmarks to the SMEFT 4F operators in terms of masses, $m_{E,U}$, and couplings, $\lambda_{E,U}$, to the SM is shown in Table 12, in the limit where all SM couplings are set to zero. We provide expressions for generic masses and couplings and in

Operator	General expression	Equal mass limit
c_{ll}	$-\frac{1}{8} \frac{1}{16\pi^2} \frac{ \lambda_E ^4}{m_E^2}$	$-\frac{1}{8} \frac{1}{16\pi^2} \frac{ \lambda_E ^4}{\Lambda^2}$
$c_{lq}^{(1)}$	$\frac{1}{8} \frac{1}{16\pi^2} \frac{ \lambda_E ^2 \lambda_U ^2 \log\left(\frac{m_E^2}{m_U^2}\right)}{m_E^2 - m_U^2}$	$\frac{1}{8} \frac{1}{16\pi^2} \frac{ \lambda_E ^2 \lambda_U ^2}{\Lambda^2}$
$c_{lq}^{(3)}$	$-\frac{1}{8} \frac{1}{16\pi^2} \frac{ \lambda_E ^2 \lambda_U ^2 \log\left(\frac{m_E^2}{m_U^2}\right)}{m_E^2 - m_U^2}$	$-\frac{1}{8} \frac{1}{16\pi^2} \frac{ \lambda_E ^2 \lambda_U ^2}{\Lambda^2}$
$c_{qq}^{(1)}$	$-\frac{1}{16} \frac{1}{16\pi^2} \frac{ \lambda_U ^4}{m_U^2}$	$-\frac{1}{16} \frac{1}{16\pi^2} \frac{ \lambda_U ^4}{\Lambda^2}$
$c_{qq}^{(3)}$	$-\frac{1}{16} \frac{1}{16\pi^2} \frac{ \lambda_U ^4}{m_U^2}$	$-\frac{1}{16} \frac{1}{16\pi^2} \frac{ \lambda_U ^4}{\Lambda^2}$

Table 12: Matching for the simple “EU” model in the limit of $\lambda_{SM} \rightarrow 0$.

the right-most column the limit for the couplings and masses being set equal at a scale $\Lambda = m_E = m_U$. The Wilson coefficients for all other 4F operators are zero in this limit, consistent with the overlap table.

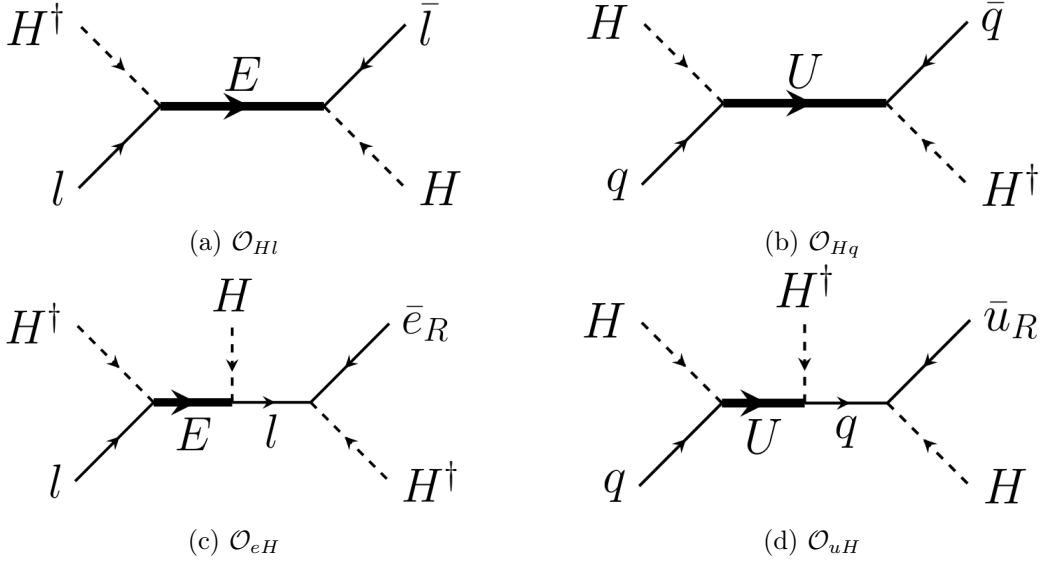


Figure 9: Diagrams for the operators \mathcal{O}_{Hl} , \mathcal{O}_{Hq} , \mathcal{O}_{eH} and \mathcal{O}_{uH} at tree-level. L and Q denote the SM lepton and quark doublet respectively.

In Table 13 we also provide the matching with the tree-level contributions of the model to Higgs-fermion couplings which would result from computing diagrams as shown in Fig. 9. Note that here we kept the SM Yukawa couplings for completeness. Thus, some of these tree-level contributions are Yukawa-suppressed and would only be relevant for the top quark.

The matching discussed above is given in the limit where all SM couplings are neglected. Whether this is a good approximation or not depends on the actual numerical value of the (unknown) BSM couplings λ_U and λ_E . In Fig. 10 we show the coefficients of two example operators multiplied by $16\pi^2\Lambda^2$ as a function of λ_U , λ_E . In the limit $\lambda_U, \lambda_E \rightarrow 1$, the corrections to the coefficients from the gauge couplings is order 40 % (10 %) in case of $\mathcal{O}_{qq}^{(1)}$

Operator	General expression
$c_{\phi l}^{(1)}$	$-\frac{1}{4} \frac{ \lambda_E ^2}{m_E^2}$
$c_{\phi l}^{(3)}$	$-\frac{1}{4} \frac{ \lambda_E ^2}{m_E^2}$
$c_{\phi q}^{(1)}$	$\frac{1}{4} \frac{ \lambda_U ^2}{m_U^2}$
$c_{\phi q}^{(3)}$	$-\frac{1}{4} \frac{ \lambda_U ^2}{m_U^2}$
$c_{e\phi}$	$\frac{1}{2} \frac{ \lambda_E ^2}{m_E^2} y_e$
$c_{u\phi}$	$\frac{1}{2} \frac{ \lambda_U ^2}{m_U^2} y_u$

Table 13: Matching for the ψH terms in the EU model. Since all coefficients depend on only one mass, the equal mass limit $m_E = m_U = \Lambda$ is trivial.

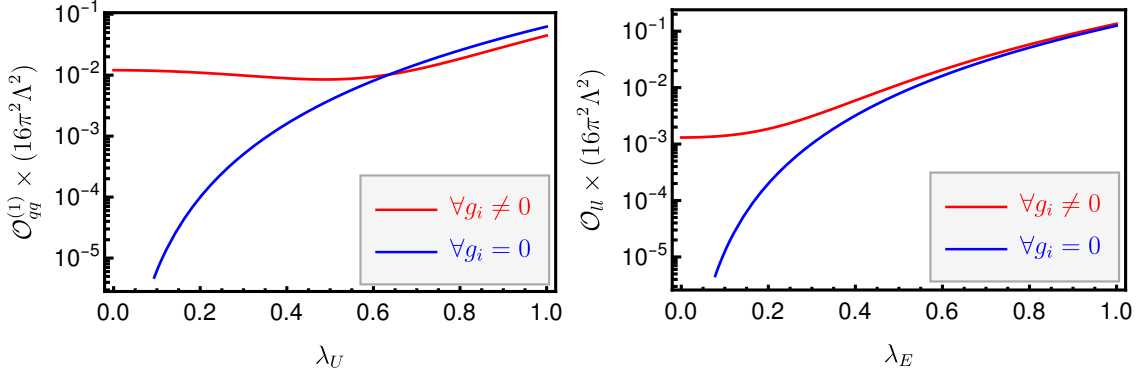


Figure 10: The coefficients for the operators $\mathcal{O}_{qq}^{(1)}$ (left) and \mathcal{O}_{ll} as a function of the new Yukawa coupling λ_U and λ_E respectively. In each case we multiply the coefficient by a factor $16\pi^2\Lambda^2$, where Λ is either M_U or M_E , common to all one-loop generated operators. The blue lines set all SM couplings to zero arbitrarily while the red lines show the calculation for g_i non-zero. For discussion see text.

(\mathcal{O}_{ll}). Both larger and smaller coefficients are possible once the g_i 's are taken into account, the relative sign depending on both the operator and the model generating it.

In summary, we have discussed some simple scenarios which produce lepton- and quark-specific 4F operators, and combining both we also have one example for a minimal hybrid model. The matching, in the limit of equal masses and couplings and in the limit of negligible gauge and Yukawa couplings, produces interesting patterns which we will explore in the next section, devoted to the interplay between direct searches at the LHC and the low-energy limits provided by former experiments. The pattern can be summarised as follows:

$$\boxed{\text{EU model pattern: } c_{ll} = -c_{lq}^{(1)} = c_{lq}^{(3)} = 2c_{qq}^{(1)} = 2c_{qq}^{(3)},}$$

whereas all the other 4F operators are not generated.

3.5 Non-minimal quark-specific scenarios

The models presented in the previous subsection are all minimal in the sense that they contain as few BSM particles as possible. One interesting scenario beyond minimality are models that only lead to 4-quark operators and do not produce any 4F operators involving leptons. These models, which evade the stronger LL and LQ constraints from low energies, are of particular interest for hadron collider searches.

Restricting ourselves to the representations $(\max SU3, \max SU2, \max Y) = (3, 2, 4)$ we find that only a small number of particles actually contributes to the models that open up the 4-quark operators. These models include SM Higgs doublets H , the fermionic exits Δ_1 , Δ_3 , U , D , E , Q_1 , Q_5 , Q_7 and the scalar exit S .

The possible decay channels of all the exits were listed in Table 7 for scalars, and in Table 8 for fermions, respectively. Note that by definition these exits always decay into two SM particles. Moreover, the models feature 14 non-exit particles which decay into one exit particle and a SM particle. The description of these new particles can be found in subsection 3.3 and their decays were listed in Tables 9 and 10.

The list of models which generate 4Q operators are shown in Appendix A, in Tables 14 and 15. Among these quark-specific models, models that produce only 4-quark operators and not any 4-lepton or 2-quark-2-lepton operator, are identified with bold symbols.

Note that more than half of the models which produce 4Q operators are also quark-specific. Therefore, from the standpoint of model building, it is natural to think of UV scenarios which would evade most low-energy constraints, and for which the LHC would be the most sensitive probe.

4 The phenomenological interplay between SMEFT indirect limits and direct searches at the LHC

So far we have discussed UV completions for 4F operators from a theoretical perspective. We have produced a list of models leading to specific 4F operators and discussed assumptions to reduce their number. For example, when we consider only representations up to triplets of color and electroweak doublets, we found that the number of possible scenarios is quite manageable. In this section we discuss some of the phenomenology that these models would produce.

4.1 Indirect searches with precise low-energy data

The first way to search for these scenarios would be through their imprint at low energies, in terms of 4F operators of the LL, LQ and QQ types. Constraints on LL [13] and LQ operators [14, 41, 42] are particularly strong as they can be probed by high-precision measurements, particularly at e^+e^- collisions, neutrino scattering and atomic parity violation experiments.

A global analysis of the constraints derived from low-energy probes in LL and LQ 4F operators was performed in [14], where the authors also provided the χ^2 in terms of the Wilson coefficients. For this work, the EFT effects in 4F are loop-suppressed by construction. Moreover, in each specific UV completion one finds relations among the coefficients

(patterns) which further restrict the form of the χ^2 function. For example, in the simple EU model described in subsection 3.4, most of the Wilson coefficients are not generated or they are suppressed by Yukawa or gauge couplings. And the coefficients that are generated are related to each other in simple ways when the new couplings and masses are set to be equal, e.g. the pattern in the EU model looks like

$$c_{ll} = -c_{lq}^{(1)} = c_{lq}^{(3)} = 2 c_{qq}^{(1)} = 2 c_{qq}^{(3)} . \quad (4.1)$$

This type of behaviour is expected from any UV completion we have considered here, as in each loop there would be 2-4 new particles and they would only generate a subset of Wilson coefficients. Patterns like the one shown above tend to produce stronger constraints on the Wilson coefficients, as one coefficient can be probed in more than one type of experiment.

In particular for the EU model, the form of the χ^2 is simple and depends on one variable

$$\chi^2(\bar{c}_{ll}) = 26.8 + 198.4 \bar{c}_{ll} + 1.42 \times 10^6 \bar{c}_{ll}^2 , \quad (4.2)$$

where we have defined $\bar{c}_{ll} = v^2 c_{ll}$, with $v = 246$ GeV [14].

Minimising $\chi^2 - \chi_{min}^2$, we obtain a 2σ limit in the parameter $\bar{c}_{ll} \in [-1.7, 1.6] \times 10^{-3}$, which translates into

$$c_{ll}^{EU} \in [-2.9, 2.7] \times 10^{-2} \text{ TeV}^{-2} . \quad (4.3)$$

4.2 Direct high-energy probes

The EFT can also be probed at high energies, exploiting the specific non-resonant kinematics they produce. In the context of the LL and LQ operators, this question was explored in [14]. Similarly, for individual QQ operators the best high-energy probes are dijet searches at the LHC [43].

In this work, though, we focus on models which induce loop-suppressed 4F operators and render much weaker indirect limits on the UV parameter space. Within these scenarios, one can explore the interplay between indirect precision searches and direct LHC resonant searches. With light resonances, the extension of the EFT approach from precision low-energy to the LHC would break down, such as the 4F analyses in Refs. [14, 43].

From all the new resonances, one should expect those with colour charge to be produced more copiously. Among the exit particles, one finds several vector-like fermion exit triplets of color, U , D , $Q_{1,5,7}$ and $T_{1,2}$, see Table 3. Inspecting the decay Tables 8 and evaluating them after electroweak symmetry breaking, one finds that the main LHC search for the UV completions would be diboson production with two energetic jets, namely

$$\begin{aligned} pp &\rightarrow hh + 2j \\ &W^\pm(Z, \gamma) + 2j \\ &W^+W^- + 2j \\ &(Z, \gamma)(Z, \gamma) + 2j , \end{aligned} \quad (4.4)$$

where one boson and one jet would reconstruct the resonance.

There are few searches in these final states, particularly focused on vector-boson fusion (VBF). For example, the di-Higgs VBF production analysis in Ref [44] would capture some of this signal but with a largely reduced sensitivity due to forward-jet cuts and veto on centrality. Another possibility would be to explore the sensitivity of diboson channels and focus on the kinematic region with two or more hard jets, e.g. reinterpreting the combination of di-Higgs searches in [45].

A copious di-Higgs production is particularly attractive, as it is a priority for LHC searches but the SM rates are very low. On the other hand, the best limits are likely to come from well-understood, high-statistics channels with W^+W^- . In particular, searches of two W-bosons with more than one hard jet should be particularly sensitive.

In [46], the channel with $e^\pm\nu\mu\mp\nu$ with at least one jet of $p_T > 30$ GeV was explored with the Run2 dataset of 139 fb^{-1} . Using the HEPDATA source on the distribution in jets and focusing on the bin with two jets, the agreement between prediction and data is at the level of 10%. This leads to a limit after cuts on the production cross-section of new particles of around 60-70 fb. Note that this limit is very rough and sub-optimal, as a dedicated search for pair production of resonances decaying into a W-boson and a jet would be more sensitive. We will nevertheless use this limit based on an existing search to illustrate the interplay of direct and indirect searches in the next subsection.

We also find several non-exist new coloured particles, see Tables 5 and 6 which would be double-produced via their strong coupling and would lead to even richer final states, namely states with two bosons and 3-4 additional objects,

$$\begin{aligned}
pp &\rightarrow \text{Diboson} + 4j \\
&\text{Diboson} + 2j + 2\ell \\
&\text{Diboson} + 2j + \ell^\pm + \text{MET} \\
&\text{Diboson} + 2j + \text{MET}.
\end{aligned}
\tag{4.5}$$

4.3 The interplay between low-energy and LHC resonant probes

We finish this section by exploring an example of the complementarity between indirect and direct probes in the loop-suppressed 4F scenarios. We choose for simplicity the minimal EU model described in subsection 3.4. For simplicity, we will also assume that all new couplings and masses are equal, which leads to simple matching expressions, cf. the right-most column in Table 12.

This model is constrained by low-energies as shown in Eq. (4.3), which translates into a rather weak 2σ constraint on the combination of model parameters, $m_{EU} > 0.17|\lambda_{EU}|^2$ TeV.

As discussed in the previous section, pairs of coloured resonances would be strongly produced, and decay to a two-boson and two-jet final state. We find that the current most-sensitive channel is the SM W^+W^- measurement at the LHC in the two-jet channel, where we find an approximate 2σ cross-section limit of 65 fb. Assuming order one branching ratio to this final state and efficiency to the experimental cuts also of order one, this limit in cross-section leads to a mass limit of the order of 650 GeV.

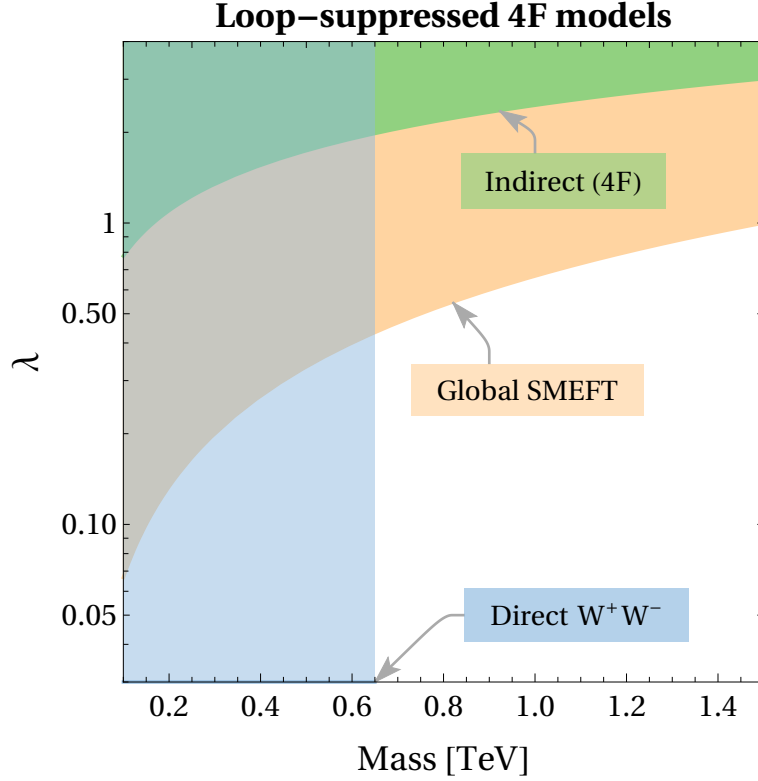


Figure 11: Interplay between indirect low-energy probes, SMEFT global fits, and resonant LHC searches for the EU benchmark.

Besides providing direct limits on resonant production, the LHC provides indirect information on new physics. In particular, global SMEFT fits using low-energy data and LHC SM precision measurements place bounds on contributions to Higgs-fermion dimension-six couplings, such as $\mathcal{O}_{\phi l}^{(1,3)}$ and $\mathcal{O}_{\phi q}^{(1,3)}$. Following the global analysis in [47] we know the bounds on SMEFT operators after marginalising over possible SMEFT contributions. In particular, we find that the most stringent limit in the set of operators $\mathcal{O}_{\phi l}^{(1,3)}$ and $\mathcal{O}_{\phi q}^{(1,3)}$ is a 2σ bound $c_{\phi q}^{(3)} \in [-0.11, +0.012] \text{ TeV}^{-2}$, with the other three operators constrained at a similar, but weaker, level.

In the EU model, the translation between operator coefficients and model parameters is shown in Table 13, leading to $m_{EU} > |\lambda_{EU}| 1.5 \text{ TeV}$, which is, as expected, much stronger than the loop-suppressed 4F limits.

The combination of the direct and indirect limits is shown in Fig. 11. From this plot, one observes that the LHC direct probes provide a better handle on scenarios with relatively small coupling $\lambda \sim 0.5$ than the SMEFT indirect probes.

We are comparing in the same mass-coupling plot indirect and direct probes, but please note that SMEFT global fits such as [16, 47] could be invalid if the observables used to set the limits were probing scales close or below m_{EU} .

It is also worth noticing that indirect probes using SM measurements at the LHC and

the LHC direct searches may not have the same scaling with luminosity. For example, one should expect that precision on diboson channels with higher jet multiplicity will improve with Run3 all the way to the HL-LHC phase, whereas the SMEFT global fits may soon saturate for the fermion-Higgs operators in Table 4, see [47] for more details.

Although Fig. 11 shows an interpretation in terms of a simple model, and we have done a rough analysis of the LHC reach, it illustrates the point that UV models with loop-suppressed 4F operators are interesting for the LHC physics case. As we have seen, these UV models contain particles with QCD coupling, unusual quantum numbers, and rich final states which motivate new types of searches.

5 Conclusions

In this paper we have focused on identifying UV scenarios leading to loop-suppressed four-fermion (4F) operators. Our motivation was to identify classes of UV models which could be discovered at the LHC, despite contributing to precise low-energy measurements.

To find these models we classified the topologies leading to loop-suppressed 4F, a task we performed using a diagrammatic approach. Although the method is general, to present our results we made various assumptions including:

- We considered UV models which do not contain a stable particle, a condition we ensure by imposing that one of the particles in the loop is an *exit* particle, namely it can decay to two SM particles. This assumption would be easily lifted to consider UV models with Dark Matter candidates.
- We focused on dimension-six operators, although our method could be used to build topologies with higher-order operators. This could be particularly interesting to identify UV completions with suppressed dimension-six operators, leading to a more dramatic energy behaviour of amplitudes, see e.g. [48] where the dimension-eight modifications of the gauge couplings are considered.
- In the phenomenological analysis we neglected SM couplings, although those contributions could be important when the new physics couplings become small, see subsection 3.4 for a brief discussion.

To connect with phenomenology, we classified the 4F operators as lepton- or quark-specific operators (those involving only leptons or quarks), and mixed operators. Low-energy limits for operators involving leptons are particularly strong, whereas quark-specific operators are especially interesting for the LHC.

We found that the typical LHC signatures of scenarios with loop-suppressed 4F operators are quite distinct, namely the production of an even number of bosons (h , W^\pm , Z and γ) and several jets and leptons. Those are new types of searches which are now motivated by the complementarity between SMEFT limits from low energies and resonances at the LHC.

To exemplify this complementarity, we provided a simple benchmark producing mixed operators and estimated the reach from the SM LHC measurement of W^+W^- in the 2 jet

bin. We found that the LHC already has a good reach, exploring areas in parameter space the low energy measurements cannot access. This naive example, based on recasting a SM measurement, suggests that dedicated searches in the multi-boson plus leptons and/or jets could reach further than our estimated 650 GeV.

Acknowledgements

We would like to acknowledge discussions with Martin Gonzalez-Alonso, Arsenii Titov and Avelino Vicente. We would also like to thank Jose Santiago for help with the tool Match-MakerEFT [30]. FE is supported by the Generalitat Valenciana with the grant GRISO-LIAP/2020/145. The research of VS is supported by the Generalitat Valenciana PROMETEO/2021/083 and the Ministerio de Ciencia e Innovacion PID2020-113644GB-I00. M.H. acknowledges support by grants PID2020-113775GB-I00 (AEI/10.13039/ 501100011033) and CIPROM/2021/054 (Generalitat Valenciana). R.C. is supported by the Alexander von Humboldt Foundation Fellowship.

A Quark specific models

We list here the models that produce 4-quark operators for $\max SU3 = 3$, $\max SU2 = 2$ and $\max Y = 4$ at one-loop level. In bold-face we denote those models which are quark-specific, namely those that do not produce any LL and LQ 4F operators. The tables actually list the particles internal to the corresponding box diagrams, therefore also H is listed, despite being part of the SM particle content.

References

- [1] S. Weinberg, *Baryon and Lepton Nonconserving Processes*, *Phys. Rev. Lett.* **43** (1979) 1566–1570.
- [2] W. Buchmuller and D. Wyler, *Effective Lagrangian Analysis of New Interactions and Flavor Conservation*, *Nucl. Phys. B* **268** (1986) 621–653.
- [3] B. Grzadkowski, M. Iskrzynski, M. Misiak, and J. Rosiek, *Dimension-Six Terms in the Standard Model Lagrangian*, *JHEP* **10** (2010) 085, [[arXiv:1008.4884](#)].
- [4] L. Lehman, *Extending the Standard Model Effective Field Theory with the Complete Set of Dimension-7 Operators*, *Phys. Rev. D* **90** (2014), no. 12 125023, [[arXiv:1410.4193](#)].
- [5] L. Lehman and A. Martin, *Low-derivative operators of the Standard Model effective field theory via Hilbert series methods*, *JHEP* **02** (2016) 081, [[arXiv:1510.00372](#)].
- [6] B. Henning, X. Lu, T. Melia, and H. Murayama, *2, 84, 30, 993, 560, 15456, 11962, 261485, ...: Higher dimension operators in the SM EFT*, *JHEP* **08** (2017) 016, [[arXiv:1512.03433](#)]. [Erratum: *JHEP* 09, 019 (2019)].
- [7] B. Gripaios and D. Sutherland, *DEFT: A program for operators in EFT*, *JHEP* **01** (2019) 128, [[arXiv:1807.07546](#)].

- [8] J. C. Criado, *BasisGen: automatic generation of operator bases*, *Eur. Phys. J. C* **79** (2019), no. 3 256, [[arXiv:1901.03501](#)].
- [9] C. W. Murphy, *Dimension-8 operators in the Standard Model Effective Field Theory*, *JHEP* **10** (2020) 174, [[arXiv:2005.00059](#)].
- [10] H.-L. Li, Z. Ren, J. Shu, M.-L. Xiao, J.-H. Yu, and Y.-H. Zheng, *Complete set of dimension-eight operators in the standard model effective field theory*, *Phys. Rev. D* **104** (2021), no. 1 015026, [[arXiv:2005.00008](#)].
- [11] H.-L. Li, Z. Ren, M.-L. Xiao, J.-H. Yu, and Y.-H. Zheng, *Complete set of dimension-nine operators in the standard model effective field theory*, *Phys. Rev. D* **104** (2021), no. 1 015025, [[arXiv:2007.07899](#)].
- [12] Y. Liao and X.-D. Ma, *An explicit construction of the dimension-9 operator basis in the standard model effective field theory*, *JHEP* **11** (2020) 152, [[arXiv:2007.08125](#)].
- [13] A. Falkowski and K. Mimouni, *Model independent constraints on four-lepton operators*, *JHEP* **02** (2016) 086, [[arXiv:1511.07434](#)].
- [14] A. Falkowski, M. González-Alonso, and K. Mimouni, *Compilation of low-energy constraints on 4-fermion operators in the SMEFT*, *JHEP* **08** (2017) 123, [[arXiv:1706.03783](#)].
- [15] A. Falkowski, M. González-Alonso, and O. Naviliat-Cuncic, *Comprehensive analysis of beta decays within and beyond the Standard Model*, *JHEP* **04** (2021) 126, [[arXiv:2010.13797](#)].
- [16] J. Ellis, M. Madigan, K. Mimasu, V. Sanz, and T. You, *Top, Higgs, Diboson and Electroweak Fit to the Standard Model Effective Field Theory*, *JHEP* **04** (2021) 279, [[arXiv:2012.02779](#)].
- [17] A. Crivellin, S. Davidson, G. M. Pruna, and A. Signer, *Renormalisation-group improved analysis of $\mu \rightarrow e$ processes in a systematic effective-field-theory approach*, *JHEP* **05** (2017) 117, [[arXiv:1702.03020](#)].
- [18] J. de Blas, J. C. Criado, M. Perez-Victoria, and J. Santiago, *Effective description of general extensions of the Standard Model: the complete tree-level dictionary*, *JHEP* **03** (2018) 109, [[arXiv:1711.10391](#)].
- [19] H.-L. Li, Y.-H. Ni, M.-L. Xiao, and J.-H. Yu, *The Bottom-Up EFT: Complete UV Resonances of the SMEFT Operators*, [arXiv:2204.03660](#).
- [20] F. Bonnet, D. Hernandez, T. Ota, and W. Winter, *Neutrino masses from higher than $d=5$ effective operators*, *JHEP* **10** (2009) 076, [[arXiv:0907.3143](#)].
- [21] F. Bonnet, M. Hirsch, T. Ota, and W. Winter, *Systematic study of the $d=5$ Weinberg operator at one-loop order*, *JHEP* **07** (2012) 153, [[arXiv:1204.5862](#)].
- [22] D. Aristizabal Sierra, A. Degee, L. Dorame, and M. Hirsch, *Systematic classification of two-loop realizations of the Weinberg operator*, *JHEP* **03** (2015) 040, [[arXiv:1411.7038](#)].
- [23] R. Cepedello, R. M. Fonseca, and M. Hirsch, *Systematic classification of three-loop realizations of the Weinberg operator*, *JHEP* **10** (2018) 197, [[arXiv:1807.00629](#)]. [Erratum: *JHEP* **06**, 034 (2019)].
- [24] S. Das Bakshi, J. Chakraborty, S. Prakash, S. U. Rahaman, and M. Spannowsky, *EFT diagrammatica: UV roots of the CP-conserving SMEFT*, *JHEP* **06** (2021) 033, [[arXiv:2103.11593](#)].
- [25] W. Naskar, S. Prakash, and S. U. Rahaman, *EFT Diagrammatica. Part II. Tracing the UV*

- origin of bosonic $D6$ CPV and $D8$ SMEFT operators, *JHEP* **08** (2022) 190, [[arXiv:2205.00910](#)].
- [26] U. Banerjee, J. Chakraborty, S. Prakash, and S. U. Rahaman, *Characters and group invariant polynomials of (super)fields: road to “Lagrangian”*, *Eur. Phys. J. C* **80** (2020), no. 10 938, [[arXiv:2004.12830](#)].
 - [27] J. Gargalionis and R. R. Volkas, *Exploding operators for Majorana neutrino masses and beyond*, *JHEP* **01** (2021) 074, [[arXiv:2009.13537](#)].
 - [28] R. M. Fonseca, *GroupMath: A Mathematica package for group theory calculations*, *Comput. Phys. Commun.* **267** (2021) 108085, [[arXiv:2011.01764](#)].
 - [29] R. M. Fonseca, *The Sym2Int program: going from symmetries to interactions*, *J. Phys. Conf. Ser.* **873** (2017), no. 1 012045, [[arXiv:1703.05221](#)].
 - [30] A. Carmona, A. Lazopoulos, P. Olgoso, and J. Santiago, *Matchmakereft: automated tree-level and one-loop matching*, *SciPost Phys.* **12** (2022), no. 6 198, [[arXiv:2112.10787](#)].
 - [31] R. M. Fonseca and M. Hirsch, *Gauge vectors and double beta decay*, *Phys. Rev. D* **95** (2017), no. 3 035033, [[arXiv:1612.04272](#)].
 - [32] C. Biggio, M. Bordone, L. Di Luzio, and G. Ridolfi, *Massive vectors and loop observables: the $g - 2$ case*, *JHEP* **10** (2016) 002, [[arXiv:1607.07621](#)].
 - [33] R. M. Fonseca, *A triplet gauge boson with hypercharge one*, [[arXiv:2205.12294](#)].
 - [34] **Particle Data Group** Collaboration, P. A. Zyla et al., *Review of Particle Physics*, *PTEP* **2020** (2020), no. 8 083C01.
 - [35] T. K. Hemmick et al., *A Search for Anomalously Heavy Isotopes of Low Z Nuclei*, *Phys. Rev. D* **41** (1990) 2074–2080.
 - [36] A. Kudo and M. Yamaguchi, *Inflation with low reheat temperature and cosmological constraint on stable charged massive particles*, *Phys. Lett. B* **516** (2001) 151–155, [[hep-ph/0103272](#)].
 - [37] M. Taoso, G. Bertone, and A. Masiero, *Dark Matter Candidates: A Ten-Point Test*, *JCAP* **03** (2008) 022, [[arXiv:0711.4996](#)].
 - [38] C. Arbeláez, R. Cepedello, J. C. Helo, M. Hirsch, and S. Kovalenko, *How many 1-loop neutrino mass models are there?*, [[arXiv:2205.13063](#)].
 - [39] F. del Aguila, M. Perez-Victoria, and J. Santiago, *Observable contributions of new exotic quarks to quark mixing*, *JHEP* **09** (2000) 011, [[hep-ph/0007316](#)].
 - [40] F. del Aguila, J. de Blas, and M. Perez-Victoria, *Effects of new leptons in Electroweak Precision Data*, *Phys. Rev. D* **78** (2008) 013010, [[arXiv:0803.4008](#)].
 - [41] M. Carpentier and S. Davidson, *Constraints on two-lepton, two quark operators*, *Eur. Phys. J. C* **70** (2010) 1071–1090, [[arXiv:1008.0280](#)].
 - [42] J. de Blas, M. Chala, and J. Santiago, *Global Constraints on Lepton-Quark Contact Interactions*, *Phys. Rev. D* **88** (2013) 095011, [[arXiv:1307.5068](#)].
 - [43] O. Domenech, A. Pomarol, and J. Serra, *Probing the SM with Dijets at the LHC*, *Phys. Rev. D* **85** (2012) 074030, [[arXiv:1201.6510](#)].
 - [44] **ATLAS** Collaboration, G. Aad et al., *Search for the $HH \rightarrow b\bar{b}b\bar{b}$ process via vector-boson fusion production using proton-proton collisions at $\sqrt{s} = 13$ TeV with the ATLAS detector*,

- JHEP* **07** (2020) 108, [[arXiv:2001.05178](#)]. [Erratum: *JHEP* 01, 145 (2021), Erratum: *JHEP* 05, 207 (2021)].
- [45] **ATLAS** Collaboration, G. Aad et al., *Combination of searches for Higgs boson pairs in pp collisions at $\sqrt{s}=13$ TeV with the ATLAS detector*, *Phys. Lett. B* **800** (2020) 135103, [[arXiv:1906.02025](#)].
- [46] **ATLAS** Collaboration, G. Aad et al., *Measurements of $W^+W^- + \geq 1$ jet production cross-sections in pp collisions at $\sqrt{s}=13$ TeV with the ATLAS detector*, *JHEP* **06** (2021) 003, [[arXiv:2103.10319](#)].
- [47] J. Ellis, C. W. Murphy, V. Sanz, and T. You, *Updated Global SMEFT Fit to Higgs, Diboson and Electroweak Data*, *JHEP* **06** (2018) 146, [[arXiv:1803.03252](#)].
- [48] C. Degrande, *A basis of dimension-eight operators for anomalous neutral triple gauge boson interactions*, *JHEP* **02** (2014) 101, [[arXiv:1308.6323](#)].

operator				
\mathcal{O}_{qq}	H	U	H	\bar{D}
	U	Π_5^\dagger	U	H
	U	H	U	H
	Q₁	S	Q₁	S
	D	H[†]	D	H[†]
	\bar{U}	Π_5	\bar{U}	Π_5
	ω_5	\bar{Q}_{11}	ω_5	$\bar{\Delta}_3$
	Π_5^\dagger	\bar{E}	Π_5^\dagger	U
	\bar{E}	Π_5^\dagger	\bar{E}	Π_5^\dagger
	Δ_3	ω_5^\dagger	Δ_3	ω_5^\dagger
\mathcal{O}_{quqd}	\bar{D}	H	U	S
	\bar{Q}_1	S	Q₁	H[†]
	Q₇	H	U	Π_5^\dagger
	\bar{D}	H	\bar{Q}_1	S
	\bar{Q}_1	S	\bar{U}	H[†]
	\bar{Q}_7	Π_{11}	\bar{X}_5	ϕ_3^\dagger
	\bar{Q}_1	Π_5	\bar{U}	H^\dagger
	Δ_3	Π_{13}^\dagger	\bar{N}_2	Π_{11}
	N_2	Π_{13}	$\bar{\Delta}_3$	ω_5
	Q_{11}	ω_5^\dagger	Δ_3	Π_{13}^\dagger
\mathcal{O}_{qd}	ϕ_3	X₅	ϕ_3	Q₇
	H	U	H	Q₁
	\bar{D}	H	Q₁	S
	\bar{Q}_5	H	U	H
	\bar{D}	S	Q₁	S
	H[†]	D	H[†]	Q₅
	Π_5	\bar{U}	Π_5	\bar{Q}_7
	\bar{D}	H	\bar{D}	S
	\bar{Q}_1	S	\bar{Q}_1	H[†]
	\bar{Q}_1	H[†]	D	H[†]
	\bar{Q}_7	ϕ_3^\dagger	X₄	ϕ_3^\dagger
	Δ_1	Π_5	\bar{U}	Π_5
	Δ_3	ω_5^\dagger	Δ_3	Π_{11}
	ω_5^\dagger	Δ_3	ω_5^\dagger	\bar{N}_2
	Δ_3	Π_{11}	\bar{X}_5	Π_{11}
	Π_{11}^\dagger	N_2	ω_5	$\bar{\Delta}_3$
	Π_{11}^\dagger	N_2	Π_{11}^\dagger	$\bar{\Delta}_3$
	Π_5^\dagger	\bar{E}	Π_5^\dagger	$\bar{\Delta}_1$
	Q_7	Π_5^\dagger	\bar{E}	Π_5^\dagger
	X_4	ω_5^\dagger	Δ_3	ω_5^\dagger

operator				
\mathcal{O}_{qu}	Π_{13}	$\bar{\Delta}_3$	Π_{13}	N₂
	ϕ_3	\bar{Q}_5	ϕ_3	\bar{X}_4
	Π_{11}^\dagger	Q₇	Π_{11}^\dagger	X₅
	\bar{X}_7	Π_{13}	$\bar{\Delta}_3$	Π_{13}
	N₂	Π_{11}^\dagger	Q₇	Π_{11}^\dagger
	H	\bar{Q}_1	H	\bar{D}
	U	S	U	H
	Q₁	H[†]	Q₁	S
	X₅	ϕ_3	\bar{Q}_5	ϕ_3
	S	\bar{U}	S	\bar{Q}_1
	H[†]	\bar{Q}_7	H[†]	\bar{U}
	U	S	\bar{Q}_1	H
	U	H	\bar{Q}_1	H
	D	H[†]	\bar{Q}_7	H[†]
	\bar{U}	S	\bar{U}	Π_5
	Δ_3	ω_5^\dagger	X_7	ω_5^\dagger
	ω_5	\bar{E}	ω_5	$\bar{\Delta}_3$
	\bar{X}_7	ω_5	$\bar{\Delta}_3$	Π_{13}
	ω_5	\bar{E}	Π_5^\dagger	$\bar{\Delta}_3$
	Π_5^\dagger	Q_1	Π_5^\dagger	U
	\bar{Q}_{11}	ω_5	\bar{E}	ω_5
	\bar{E}	Π_5^\dagger	Q_1	Π_5^\dagger
	\bar{E}	ω_5	\bar{E}	Π_5^\dagger
	Q_1	Π_5^\dagger	Q_1	S
	Π_5^\dagger	Q_1	S	U
	Π_5	Δ_3	Π_5	E
	Δ_3	Π_{13}^\dagger	Δ_3	ω_5^\dagger
	\bar{U}	Π_5	Δ_3	Π_5
	Δ_3	Π_5	Δ_3	ω_5^\dagger

Table 14: Quark specific models, part 1. Boldface models are quark-specific.

operator				
\mathcal{O}_{uu}	Π_{13}	$\bar{\Delta}_3$	Π_{13}	\bar{Q}_{17}
	ϕ_3	\bar{Q}_5	ϕ_3	Q_{13}
	Π_{11}^\dagger	Q_7	Π_{11}^\dagger	Δ_5
	Q_7	H	Q_7	Π_{11}^\dagger
	$\bar{\Delta}_3$	Π_{13}	$\bar{\Delta}_3$	Π_{13}
	Q_7	Π_{11}^\dagger	Q_7	Π_{11}^\dagger
	H	\bar{Q}_1	H	Q_7
	\bar{Q}_5	ϕ_3	\bar{Q}_5	ϕ_3
	S	\bar{U}	S	U
	\bar{Q}_1	H	\bar{Q}_1	H
	Q_7	H^\dagger	Q_7	H^\dagger
	ω_5	\bar{E}	ω_5	\bar{X}_7
	$\bar{\Delta}_3$	Π_5^\dagger	$\bar{\Delta}_3$	Π_{13}
	Π_5^\dagger	Q_1	Π_5^\dagger	$\bar{\Delta}_3$
	Q_1	H^\dagger	Q_1	Π_5^\dagger
	\bar{E}	ω_5	\bar{E}	ω_5
	Q_1	Π_5^\dagger	Q_1	Π_5^\dagger
	Δ_3	Π_5	Δ_3	Π_5
\mathcal{O}_{dd}	ϕ_3	\bar{Q}_{11}	ϕ_3	Q_7
	Q_7	ϕ_3	Q_7	Π_5^\dagger
	Q_7	Π_5^\dagger	Q_7	Π_5^\dagger
	H	\bar{Q}_5	H	Q_1
	\bar{Q}_5	H	\bar{Q}_5	H
	S	\bar{D}	S	D
	\bar{Q}_1	H^\dagger	\bar{Q}_1	H^\dagger
	\bar{Q}_7	ϕ_3^\dagger	\bar{Q}_7	ϕ_3^\dagger
	Π_{11}^\dagger	Q_{13}	Π_{11}^\dagger	$\bar{\Delta}_3$
	Π_5^\dagger	Q_7	Π_5^\dagger	$\bar{\Delta}_1$
	Δ_1	Π_5	Δ_1	Π_5
	Δ_3	Π_{11}	Δ_3	Π_{11}

operator				
\mathcal{O}_{ud}	Π_{13}	$\bar{\Delta}_3$	Π_{13}	\bar{Q}_{11}
	ϕ_3	\bar{Q}_5	ϕ_3	Q_7
	Q_{13}	ϕ_3	Q_7	Π_{11}^\dagger
	Q_7	H	Q_7	Π_5^\dagger
	Δ_5	Π_{13}	$\bar{\Delta}_3$	Π_{13}
	Q_{13}	Π_{11}^\dagger	Q_7	Π_{11}^\dagger
	Q_7	Π_{11}^\dagger	Q_7	Π_5^\dagger
	ϕ_3	\bar{Q}_5	H	Q_7
	H	\bar{Q}_1	H	Q_1
	\bar{Q}_{11}	ϕ_3	\bar{Q}_5	ϕ_3
	\bar{Q}_5	ϕ_3	\bar{Q}_5	H
	S	\bar{U}	S	D
	H^\dagger	\bar{Q}_7	H^\dagger	Q_5
	\bar{Q}_5	H	\bar{Q}_1	H
	\bar{Q}_7	Π_{11}	\bar{Q}_7	ϕ_3^\dagger
	\bar{Q}_1	H^\dagger	\bar{Q}_7	H^\dagger
	\bar{Q}_7	H^\dagger	\bar{Q}_7	ϕ_3^\dagger
	\bar{Q}_7	ϕ_3^\dagger	\bar{Q}_{13}	ϕ_3^\dagger
	ω_5	\bar{E}	ω_5	\bar{X}_4
	Π_{11}^\dagger	Q_7	Π_{11}^\dagger	$\bar{\Delta}_3$
	Δ_5	Π_{11}^\dagger	$\bar{\Delta}_3$	Π_{13}
	Π_{11}^\dagger	Q_7	Π_5^\dagger	$\bar{\Delta}_3$
	Π_5^\dagger	Q_1	Π_5^\dagger	Δ_1^\dagger
	Q_7	H	Q_1	Π_5^\dagger
	N_2	ω_5	\bar{E}	ω_5
	Q_7	Π_5^\dagger	Q_1	Π_5^\dagger
	Π_5	Δ_3	Π_5	\bar{Q}_7
	\bar{Q}_1	Π_5	\bar{Q}_1	H^\dagger
	Δ_3	Π_{13}^\dagger	Δ_3	Π_{11}
	Δ_1	Π_5	Δ_3	Π_5
	Δ_3	Π_5	Δ_3	Π_{11}
	Δ_3	Π_{11}	$\bar{\Delta}_5$	Π_{11}

Table 15: Quark specific models, part 2. Boldface models are quark-specific.